EUROPEAN ORGANIZATION FOR NUCLEAR RESEARCH

CERN-EP/2000-130
October 10, 2000

Search for R-parity Violating Decays of Supersymmetric Particles in e^+e^- Collisions at $\sqrt{s} = 189$ GeV

The L3 Collaboration

Abstract

A search for chargino, neutralino and scalar lepton pair-production in e^+e^- collisions at the centre-of-mass energy of 189 GeV is performed under the assumptions that R-parity is not conserved in decays and only one of the coupling constants λ_{ijk}, λ'_{ijk} or λ''_{ijk} is non-negligible. No signal is found in a data sample corresponding to an integrated luminosity of 176.4 pb^{-1}. Limits on the production cross sections, on the Minimal Supersymmetric Standard Model parameters and on the masses of the supersymmetric particles are derived.

Submitted to *Eur. Phys. J.*

1 Introduction

The most general superpotential of the Minimal Supersymmetric Standard Model (MSSM) [1], which describes a supersymmetric, renormalizable and gauge invariant theory, with minimal particle content, includes the term $\mathrm{W_R}$ [2,3]:

$$\mathrm{W_R} = \lambda_{ijk}\mathrm{L}_i\mathrm{L}_j\overline{\mathrm{E}}_k + \lambda'_{ijk}\mathrm{L}_i\mathrm{Q}_j\overline{\mathrm{D}}_k + \lambda''_{ijk}\overline{\mathrm{U}}_i\overline{\mathrm{D}}_j\overline{\mathrm{D}}_k\,, \tag{1}$$

where λ_{ijk}, λ'_{ijk} and λ''_{ijk} are the Yukawa couplings and i, j and k the generation indices; L_i and Q_i are the left-handed lepton- and quark-doublet superfields, $\overline{\mathrm{E}}_i$, $\overline{\mathrm{D}}_i$ and $\overline{\mathrm{U}}_i$ are the right-handed singlet superfields for charged leptons, down- and up-type quarks, respectively. In order to prevent the simultaneous presence of identical fermionic fields, the following antisymmetry relations are required: $\lambda_{ijk} = -\lambda_{jik}$ and $\lambda''_{ijk} = -\lambda''_{ikj}$, reducing to $9+27+9$ the total number of independent Yukawa couplings. The $\mathrm{L}_i\mathrm{L}_j\overline{\mathrm{E}}_k$ and $\mathrm{L}_i\mathrm{Q}_j\overline{\mathrm{D}}_k$ terms violate the leptonic quantum number L, while the $\overline{\mathrm{U}}_i\overline{\mathrm{D}}_j\overline{\mathrm{D}}_k$ terms violate the baryonic quantum number B.

The simultaneous presence of L- and B-violating terms would lead to a fast proton decay[1)] [4]. Therefore, existing limits [5] on the proton lifetime require either of two possibilities.

The first one is to impose R-parity conservation, which forbids all terms in Equation 1. R-parity is a multiplicative quantum number defined as:

$$\mathrm{R} = (-1)^{3\mathrm{B}+\mathrm{L}+2\mathrm{S}}\,, \tag{2}$$

where S is the spin. R is $+1$ for all ordinary particles, and -1 for their supersymmetric partners. If R-parity is conserved, supersymmetric particles can be produced only in pairs and they decay in cascade to the lightest supersymmetric particle (LSP), which is stable [6].

The second possibility is considered in this paper. Since the absence of either the B-violating or the L-violating terms is enough to prevent a fast proton decay, there is no need to impose *a priori* R-parity conservation. As a consequence, two new kinds of processes are allowed: single production of supersymmetric particles, or LSP decays into Standard Model particles via scalar lepton or quark exchange. In the latter case, the MSSM production mechanisms are unaltered by the operators in Equation 1.

In this paper, we describe the search for pair-produced neutralinos[2)] ($\mathrm{e^+e^-} \rightarrow \tilde{\chi}^0_m\tilde{\chi}^0_n$, with $m = 1,2$ and $n = 1,..,4$), charginos ($\mathrm{e^+e^-} \rightarrow \tilde{\chi}^+_1\tilde{\chi}^-_1$) and scalar leptons ($\mathrm{e^+e^-} \rightarrow \tilde{\ell}^+_R\tilde{\ell}^-_R$, $\mathrm{e^+e^-} \rightarrow \tilde{\nu}\tilde{\nu}$) with subsequent R-parity violating decays, assuming that only one of the coupling constants λ_{ijk}, λ'_{ijk} or λ''_{ijk} is non-negligible. Only $\tilde{\ell}_R$ (supersymmetric partners of the right-handed charged leptons) are considered in this analysis, since they are expected to be lighter than the corresponding left-handed ones.

Supersymmetric particles can decay directly into two or three fermions according to the dominant interaction term, as detailed in Table 1. Indirect decays via the LSP can occur as well. Four-body decays of the lightest scalar lepton are also taken into account in the case of λ'_{ijk} and λ''_{ijk}. In the present analysis, the dominant coupling is assumed to be greater than 10^{-5} [8], corresponding to decay lengths less than 1 cm. Previous L3 results on λ_{ijk} and λ''_{ijk} Yukawa couplings can be found in Reference 9. Searches for R-parity violating decays of supersymmetric particles were also performed by other LEP experiments [10].

---

1) With contributions at the tree level from $\lambda'_{11k}\lambda''_{11k}$, and at one-loop level from any product $\lambda_{ijk}\lambda''_{lmn}$ or $\lambda'_{ijk}\lambda''_{lmn}$.

2) Single production of supersymmetric particles is not considered in this paper.

Particle	Direct decays			Indirect decays	
	λ_{ijk}	λ'_{ijk}	λ''_{ijk}	via $\tilde{\chi}^0_1$	via $\tilde{\ell}$
$\tilde{\chi}^0_1$	$\ell^-_i \nu_j \ell^+_k$, $\nu_i \ell^+_j \ell^-_k$	$\ell^-_i \mathrm{u}_j \bar{\mathrm{d}}_k$, $\nu_i\, \mathrm{d}_j \bar{\mathrm{d}}_k$	$\bar{\mathrm{u}}_i \bar{\mathrm{d}}_j \bar{\mathrm{d}}_k$	$-$	$\ell\tilde{\ell}$
$\tilde{\chi}^0_{n(n\geq 2)}$	$\ell^-_i \nu_j \ell^+_k$, $\nu_i \ell^+_j \ell^-_k$	$\ell^-_i \mathrm{u}_j \bar{\mathrm{d}}_k$, $\nu_i\, \mathrm{d}_j \bar{\mathrm{d}}_k$	$\bar{\mathrm{u}}_i \bar{\mathrm{d}}_j \bar{\mathrm{d}}_k$	$\mathrm{Z}^*\tilde{\chi}^0_1$, $\mathrm{Z}^*\tilde{\chi}^0_{m(m<n)}$, $\mathrm{W}^*\tilde{\chi}^\pm_1$	$\ell\tilde{\ell}$
$\tilde{\chi}^+_1$	$\nu_i \nu_j \ell^+_k$, $\ell^+_i \ell^+_j \ell^-_k$	$\nu_i u_j \bar{\mathrm{d}}_k$, $\ell^+_i \bar{\mathrm{d}}_j \mathrm{d}_k$	$\bar{\mathrm{d}}_i \bar{\mathrm{d}}_j \bar{\mathrm{d}}_k$, $\mathrm{u}_i \mathrm{u}_j \mathrm{d}_k$, $\mathrm{u}_i \mathrm{d}_j \mathrm{u}_k$	$\mathrm{W}^*\tilde{\chi}^0_1$, $\mathrm{W}^*\tilde{\chi}^0_2$	
$\tilde{\ell}^-_{kR}$	$\nu_i \ell^-_j$, $\nu_j \ell^-_i$	$-$	$-$	$\ell^-_k \tilde{\chi}^0_1$	$-$
$\tilde{\nu}_i$, $\tilde{\nu}_j$	$\ell^-_j \ell^+_k$, $\ell^-_i \ell^+_k$	$-$	$-$	$\nu_i \tilde{\chi}^0_1$, $\nu_j \tilde{\chi}^0_1$	

Table 1: R-parity violating decays of the supersymmetric particles considered in this analysis. Charged conjugate states are implied. Indirect decays via scalar leptons are relevant only for neutralinos when the scalar lepton is the LSP. Only supersymmetric partners of the right-handed charged leptons are taken into account. Decays to more than three fermions are not listed. Z^* and W^* indicate virtual Z and W.

2 Data and Monte Carlo Samples

The data used correspond to an integrated luminosity of 176.4 pb^{-1} collected by the L3 detector [11] at the centre-of-mass energy ($\sqrt{s}$) of 189 GeV.

The signal events are generated with the program `SUSYGEN` [12] for different mass values and for all possible choices of the generation indices.

The following Monte Carlo generators are used to simulate Standard Model background processes: `PYTHIA` [13] for $\mathrm{e}^+\mathrm{e}^- \rightarrow \mathrm{q}\bar{\mathrm{q}}$, $\mathrm{e}^+\mathrm{e}^- \rightarrow \mathrm{Z}\,\mathrm{e}^+\mathrm{e}^-$ and $\mathrm{e}^+\mathrm{e}^- \rightarrow \mathrm{ZZ}$, `BHWIDE` [14] for $\mathrm{e}^+\mathrm{e}^- \rightarrow \mathrm{e}^+\mathrm{e}^-$, `KORALZ` [15] for $\mathrm{e}^+\mathrm{e}^- \rightarrow \mu^+\mu^-$ and $\mathrm{e}^+\mathrm{e}^- \rightarrow \tau^+\tau^-$, `PHOJET` [16] and `PYTHIA` for $\mathrm{e}^+\mathrm{e}^- \rightarrow \mathrm{e}^+\mathrm{e}^-$ hadrons, `DIAG36` [17] for $\mathrm{e}^+\mathrm{e}^- \rightarrow \mathrm{e}^+\mathrm{e}^-\ell^+\ell^-$ ($\ell = \mathrm{e}, \mu, \tau$), `KORALW` [18] for $\mathrm{e}^+\mathrm{e}^- \rightarrow \mathrm{W}^+\mathrm{W}^-$ and `EXCALIBUR` [19] for $\mathrm{e}^+\mathrm{e}^- \rightarrow \mathrm{W}^\pm\,\ell^\mp\nu$. The number of simulated events corresponds to at least 50 times the luminosity of the data, except for Bhabha and two-photon processes, where the Monte Carlo samples correspond to 2 to 6 times the luminosity.

The detector response is simulated using the `GEANT` package [20]. It takes into account effects of energy loss, multiple scattering and showering in the detector materials. Hadronic interactions are simulated with the `GHEISHA` program [21]. Time dependent inefficiencies of the different subdetectors are also taken into account in the simulation procedure.

3 Event reconstruction

Leptons ($\ell = \mathrm{e}, \mu, \tau$) and hadronic jets are reconstructed as follows. An electron is defined as an electromagnetic shower, with energy greater than 1 GeV, matched with a track in the central chamber. Muon identification requires a track in the muon chambers matched with a track in the central chamber. Hadronic tau decays are reconstructed from narrow isolated hadronic jets with energy greater than 2 GeV and one to three associated tracks. The tau energy must be contained in a cone of 10° half-opening angle around the jet direction. No additional tracks and no more than two additional calorimetric clusters are required in a further cone of 30° half-opening angle. The ratio of the energies in the two cones has to be less than 2.0. Remaining clusters and tracks are classified as hadrons. Jets are reconstructed with the DURHAM algorithm [22]. The jet resolution parameter y_{mn} is defined as the y_{cut} value at which the event configuration changes from n to m jets. N_{jets8} is the number of jets clustered with y_{cut} fixed and equal to 0.008. The acollinearity (θ_{acol}) and acoplanarity (θ_{acop}) angles are calculated by forcing hadronic and leptonic objects in every event into exactly two jets. At least one time of flight measurement has to be consistent with the beam crossing to reject cosmic rays.

4 λ_{ijk} Analysis

Table 2 shows the possible topologies arising when the λ_{ijk} couplings dominate. The different selections can be classified into four categories as follows: $2\ell + \not{E}$, $4\ell + \not{E}$, 6ℓ, $(\geq 4)\,\ell$ plus possible jets and $\not{E}$. $\not{E}$ (missing energy) indicates final state neutrinos escaping detection. After a common preselection, a dedicated selection is developed for each group, taking into account lepton flavours, particle boosts and virtual W and Z decay products.

Direct decays	Selections
$e^+e^- \to \tilde{\chi}^0_m\tilde{\chi}^0_n \to \quad \ell\ell\ell\nu\nu$	$4\,\ell + \not{E}$
$e^+e^- \to \tilde{\chi}^+_1\tilde{\chi}^-_1 \to \quad \ell\ell\ell\ell\ell\ell$ $\ell\ell\ell\ell\nu\nu$ $\ell\ell\nu\nu\nu\nu$	$6\,\ell$ $4\,\ell + \not{E}$ $2\,\ell + \not{E}$
$e^+e^- \to \tilde{\ell}^+_R\tilde{\ell}^-_R \to \quad \ell\nu\ell\nu$	$2\,\ell + \not{E}$
$e^+e^- \to \tilde{\nu}\tilde{\nu} \quad \to \quad \ell\ell\ell\ell$	$4\,\ell + \not{E}$
Indirect decays	
$e^+e^- \to \tilde{\chi}^0_m\tilde{\chi}^0_{n(n\geq 2)} \to$ cascades	$(\geq 4)\,\ell$ + (jets) + $\not{E}$
$e^+e^- \to \tilde{\chi}^+_1\tilde{\chi}^-_1 \to \quad \tilde{\chi}^0_{1(2)}\tilde{\chi}^0_{1(2)}W^*W^*$	$(\geq 4)\,\ell$ + (jets) + $\not{E}$
$e^+e^- \to \tilde{\ell}^+_R\tilde{\ell}^-_R \to \quad \ell\ell\ell\ell\ell\ell\nu\nu$	$(\geq 4)\,\ell$ + (jets) + $\not{E}$
$e^+e^- \to \tilde{\nu}\tilde{\nu} \quad \to \quad \ell\ell\ell\ell\nu\nu\nu\nu$	$4\,\ell + \not{E}$

Table 2: Processes considered in the λ_{ijk} coupling analysis and corresponding selections. $\tilde{\chi}^0_m\tilde{\chi}^0_n$ indicates neutralino pair-production with $m = 1, 2$ and $n = 1, .., 4$. "Cascades" refers to all possible final state combinations of Table 1.

Events are preselected by requiring at least two charged leptons ($N_{e,\mu,\tau}$), to reject $q\bar{q}$ events and hadronic W^+W^- and ZZ decays. Events have to contain at least 3 charged tracks (N_{tracks}) and 4 calorimetric clusters ($N_{clusters}$) in order to remove $e^+e^- \to e^+e^-, \mu^+\mu^-$ and purely leptonic $\tau^+\tau^-$ and W^+W^- decays. The visible energy (E_{vis}) is required to be less than 90% of $\sqrt{s}$, in order to reject background from lepton pair-production. If the number of tracks is at least 5, the cut on the visible energy is not applied, otherwise it would suppress signal events with six charged leptons. Back-to-back events, in particular $\tau^+\tau^-$, are reduced by requiring y_{34} to be greater than 0.0002. For low multiplicity signal events belonging to the $2\ell + \not{E}$ topologies, the following cuts are applied: events must have at least 2 and less than 6 tracks, between 2 and 15 calorimetric clusters, the visible energy has to be less than 60% of $\sqrt{s}$ and N_{jets8} has to be at least 2. In this case, the preselection requirement on y_{34} is not applied. In addition, for the $2\ell + \not{E}$ topologies, the acollinearity and acoplanarity angles are required to be below 176° in order to reject $\ell^+\ell^-$ background.

Untagged two-photon interactions are removed by requiring the visible energy to be greater than 20% of $\sqrt{s}$. The polar angle (θ_{miss}) of the missing momentum vector has to be between 15° and 165°. Background from two-photon interactions is further reduced by requiring the missing transverse momentum (p^T_{miss}) to be greater than 7 GeV. Tagged two-photon interactions are rejected by requiring the sum of the energies measured in the small angle calorimeters between 1.5° and 9.0° to be less than 10 GeV.

After the preselection is applied, 995 events are selected in the data sample and 984 ± 6 events are expected from Standard Model processes, of which 398 are from $\mathrm{W^+W^-}$, 136 from $\mathrm{W^\pm e^\mp \nu}$ decays and 258 from $\mathrm{q\bar{q}}$ events. Figure 1 shows the number of leptons, acollinearity, normalised visible energy and $\ln(y_{34})$ distributions after the preselection. The data are in good agreement with the Monte Carlo expectations.

The four groups of final selections are shown in Tables 10 to 13 of Appendix A. The efficiencies are summarized in Tables 3 and 4. Here and in the following sections we discuss only the results obtained for those choices of the generation indices which give the lowest selection efficiencies. In this way, the quoted results will be conservatively valid for any ijk combination. In the case of direct R-parity violating decays, the efficiencies are estimated for different mass values of the pair-produced supersymmetric particles. In the case of indirect decays, the efficiencies are estimated for different masses and ΔM ranges. ΔM is defined as the mass difference $M_{susy} - M_{\tilde{\chi}^0_1}$, where M_{susy} can assume different values according to the type of supersymmetric particle whose decay is considered.

In the case of direct neutralino or chargino decays, the lowest efficiencies are found for $\lambda_{ijk} = \lambda_{133}$, due to the presence of taus in the final state. The efficiencies increase with the neutralino or chargino mass. At high masses (greater than 50 GeV), six fermions are expected to be isotropically produced and can be disentangled from W pair-production background events. For low masses, the signal signatures look like back-to-back jet events and the selection efficiencies are smaller due to cuts to reduce the dominant background coming from the two-fermion processes. In addition, the efficiencies obtained for low masses are higher for charginos than for neutralinos due to the contribution of the six charged lepton final state.

For indirect chargino decays and for a chargino mass of 94 GeV, the efficiencies decrease with increasing ΔM. At high ΔM, the signal signatures are very similar to those of W pair-production. For $M_{\tilde{\chi}^0_m} + M_{\tilde{\chi}^0_n} = 188$ GeV, the efficiencies of the process $\mathrm{e^+e^-} \rightarrow \tilde{\chi}^0_m \tilde{\chi}^0_n$ ($m = 1, 2$, $n = 2, 3, 4$) decrease slightly with increasing ΔM.

In the case of pair-production of scalar charged leptons, followed by direct decays via λ_{ijk}, the final state contains two leptons plus missing energy. The lepton flavours are given by the indices i and j, independently of the value of k, as shown in Table 1. The lowest selection efficiency is found for $\lambda_{ijk} = \lambda_{12k}$, *i.e.* for events with electrons and/or muons in the final state. This is due to the fact that it is necessary, in order to reject a potential large background from lepton pair-production, to select events with at least 3 calorimetric clusters and with visible energy below 55% of $\sqrt{s}$ (Table 11). For this reason, events with lower multiplicity coming from λ_{12k} mediated decays are selected with lower efficiency. The efficiency increases with increasing scalar lepton mass.

Direct decays of scalar neutrinos provide four leptons in the final state. In this case we have used the $4\ell + \not{E}$ and $(\geq 4)\,\ell +$ (jets) $+\not{E}$ selections, without developing a dedicated one, since these selections provide, also for 4ℓ events, a good analysis sensitivity comparable to that of the dedicated selections for scalar electrons, muons and taus. Events with scalar neutrino decays into electrons and muons are thus selected with lower efficiency than events with decays into taus. In particular, the smallest efficiency is obtained for λ_{121}, which can give rise to the decays $\tilde{\nu}_e \rightarrow \mu^- e^+$ and $\tilde{\nu}_\mu \rightarrow e^- e^+$. This effect is due to the selection requirements on the energy in the electromagnetic calorimeter, which are optimized for selecting events with $4\ell + \not{E}$.

Indirect decays of charged scalar leptons ($\tilde{\ell}^+_R \tilde{\ell}^-_R \rightarrow \ell^+ \ell^- \tilde{\chi}^0_1 \tilde{\chi}^0_1$) provide six leptons plus missing energy in the final state. The events are selected by means of the $(\geq 4)\ \ell +$ (jets) $+\not{E}$ selections. Table 4 shows the efficiencies for scalar electron, muon and tau pair-production, for different values of $\Delta M = M_{\tilde{\ell}_R} - M_{\tilde{\chi}^0_1}$. For large values of ΔM the selection efficiencies are smaller for $\tilde{e}^+_R \tilde{e}^-_R$ than for the other channels because of the cut on the energy in the electromagnetic calorimeter.

Indirect decays of scalar neutrinos ($\tilde{\nu}\tilde{\nu} \rightarrow \nu\nu \tilde{\chi}^0_1 \tilde{\chi}^0_1$) are selected by the $4\ell + \not{E}$ selections. The efficiency decreases with increasing ΔM, when the two additional neutrinos can carry a relevant fraction of the total energy.

Direct decays		Mass values		
Coupling	Process	M = 5–20 GeV	M = 25–50 GeV	M=55–94 GeV
λ_{133}	$\tilde{\chi}^0_m \tilde{\chi}^0_n$	4%–13%	21%–35%	41%–51%
λ_{133}	$\tilde{\chi}^+_1 \tilde{\chi}^-_1$	8%–10%	15%–36%	43%–45%
λ'_{311}	$\tilde{\chi}^0_m \tilde{\chi}^0_n$, $\tilde{\chi}^+_1 \tilde{\chi}^-_1$	6%–17%	19%–28%	21%–26%
λ''_{212}	$\tilde{\chi}^0_m \tilde{\chi}^0_n$, $\tilde{\chi}^+_1 \tilde{\chi}^-_1$	–	29%–38%	35%–54%
Indirect decays		ΔM values		
Coupling	Process	ΔM = 5–20 GeV	ΔM = 25–50 GeV	ΔM = 55–80 GeV
λ_{133}	$\tilde{\chi}^0_m \tilde{\chi}^0_{n(n\geq 2)}$	50%–51%	48%–50%	42%–46%
λ_{133}	$\tilde{\chi}^+_1 \tilde{\chi}^-_1$	47%–59%	33%–43%	14%–27%
λ'_{311}	$\tilde{\chi}^+_1 \tilde{\chi}^-_1$	25%–28%	29%–30%	17%–23%
λ''_{212}	$\tilde{\chi}^0_m \tilde{\chi}^0_{n(n\geq 2)}$	55%–59%	59%–60%	47%–53%
λ''_{212}	$\tilde{\chi}^+_1 \tilde{\chi}^-_1$	54%–62%	60%–66%	43%–56%

Table 3: Efficiency ranges for neutralino and chargino production. $\tilde{\chi}^0_m \tilde{\chi}^0_n$ indicates neutralino pair-production with $m = 1, 2$ and $n = 1, .., 4$. The efficiencies correspond to $M_{\tilde{\chi}^0_m} + M_{\tilde{\chi}^0_n} = 188$ GeV. For direct decays the lowest mass values considered are $M_{\tilde{\chi}^0_1} = 5$ GeV and $M_{\tilde{\chi}^\pm_1} = 15$ GeV for λ_{133}, $M = 15$ GeV for λ'_{311} and $M_{\tilde{\chi}^0_1} = 20$ GeV and $M_{\tilde{\chi}^\pm_1} = 45$ GeV for λ''_{212}. For direct neutralino decays we quote the $\tilde{\chi}^0_1 \tilde{\chi}^0_1$ efficiencies. In the case of indirect decays the chargino selection efficiencies correspond to $M_{\tilde{\chi}^\pm_1} = 94$ GeV.

Direct decays		Mass values		
Coupling	Process	M = 5–20 GeV	M = 25–50 GeV	M=55–94 GeV
λ_{12k}	$\tilde{\ell}^+_R\tilde{\ell}^-_R$	–	–	8%–18%
λ_{121}	$\tilde{\nu}\tilde{\nu}$	–	–	6%–8%
λ'_{311}	$\tilde{e}^+_R\tilde{e}^-_R$ *	–	14%–16%	18%–22%
λ''_{212}	$\tilde{e}^+_R\tilde{e}^-_R$ *	–	32%–38%	35%–54%
λ''_{212}	$\tilde{\mu}^+_R\tilde{\mu}^-_R$ *	–	32%–38%	35%–54%
λ''_{212}	$\tilde{\tau}^+_R\tilde{\tau}^-_R$ *	–	32%–38%	15%–44%
Indirect decays		ΔM values		
Coupling	Process	ΔM = 5–20 GeV	ΔM = 25–50 GeV	ΔM = 55–80 GeV
λ_{133}	$\tilde{e}^+_R\tilde{e}^-_R$	74%–74%	50%–63%	26%–38%
λ_{133}	$\tilde{\mu}^+_R\tilde{\mu}^-_R$	82%–84%	76%–84%	65%–72%
λ_{133}	$\tilde{\tau}^+_R\tilde{\tau}^-_R$	66%–72%	67%–73%	57%–65%
λ_{133}	$\tilde{\nu}\tilde{\nu}$	52%–52%	39%–49%	28%–37%
λ'_{311}	$\tilde{e}^+_R\tilde{e}^-_R$	30%–60%	50%–60%	60%–76%
λ''_{212}	$\tilde{e}^+_R\tilde{e}^-_R$	37%–63%	66%–69%	45%–62%
λ''_{212}	$\tilde{\mu}^+_R\tilde{\mu}^-_R$	29%–51%	54%–57%	34%–50%
λ''_{212}	$\tilde{\tau}^+_R\tilde{\tau}^-_R$	56%–66%	39%–62%	15%–16%

Table 4: Efficiency ranges for scalar lepton production. In the case of direct decays the lowest mass value considered is $M_{\tilde{\ell}_R} = 54$ GeV for λ_{12k}, $M_{\tilde{\nu}} = 54$ GeV for λ_{121}, $M_{\tilde{e}_R} = 45$ GeV for λ'_{311} and $M_{\tilde{\ell}_R} = 30$ GeV for λ''_{212}. For the processes marked with * we refer to four-body decays, as described in Sections 5 and 6. For indirect decays the scalar lepton selection efficiencies correspond to $M_{\tilde{\ell}_R}\,(M_{\tilde{\nu}}) = 94$ GeV.

5 λ'_{ijk} Analysis

Table 5 shows the topologies arising when the λ'_{ijk} couplings dominate, as well as the different final states, classified into five categories. The quark flavour composition is given by the j and k generation indices of the dominant λ'_{ijk} coupling. After a common preselection, a dedicated selection is developed for each group, taking into account lepton flavours and charge, particle boosts and virtual Z and W decay products.

Direct decays	Selections
$e^+e^- \to \tilde{\chi}^0_m \tilde{\chi}^0_n \ \to$ qqqq $\ell\ell$	4 jets + 2 ℓ
qqqq $\ell\nu$	4 jets + ℓ + $\not{E}$
qqqq $\nu\nu$	4 jets + $\not{E}$
$e^+e^- \to \tilde{\chi}^+_1 \tilde{\chi}^-_1 \ \to$ qqqq $\ell\ell$	4 jets + 2 ℓ
qqqq $\ell\nu$	4 jets + ℓ + $\not{E}$
qqqq $\nu\nu$	4 jets + $\not{E}$
Indirect decays	
$e^+e^- \to \tilde{\chi}^0_m \tilde{\chi}^0_{n(n\geq 2)} \ \to$ cascades	multijets (+ leptons) (+ $\not{E}$)
$e^+e^- \to \tilde{\chi}^+_1 \tilde{\chi}^-_1 \ \to \ \tilde{\chi}^0_{1(2)} \tilde{\chi}^0_{1(2)} W^* W^*$	multijets (+ leptons) (+ $\not{E}$)
$e^+e^- \to \tilde{e}^+_R \tilde{e}^-_R \ \to \ \tilde{\chi}^0_1 \tilde{\chi}^0_1$ ee	4 jets + 2–4 ℓ (+ $\not{E}$)

Table 5: Processes considered in the λ'_{ijk} coupling analysis and corresponding selections. For masses below 50 GeV or small ΔM values not all jets in the event can be resolved. $\tilde{\chi}^0_m \tilde{\chi}^0_n$ indicates neutralino pair-production with $m = 1, 2$ and $n = 1, .., 4$. "Cascades" refers to all possible final state combinations of Table 1.

Events are preselected by requiring at least 4 charged tracks and 5 calorimetric clusters in order to remove $e^+e^- \to e^+e^-, \mu^+\mu^-$ and purely leptonic $\tau^+\tau^-$ and W^+W^- decays. For centre-of-mass energies above the Z peak a large fraction of background events contains a hard initial state radiation (ISR) photon. In order to remove these events the polar angle of the missing momentum has to be between 7° and 173°.

Untagged two-photon interactions are removed by requiring the energy in a cone of 12° half-opening angle around the beam axis not to exceed 20% of the total visible energy. In addition, the visible energy must be greater than 30% of $\sqrt{s}$. Tagged two-photon interactions are rejected as explained in Section 4.

In this analysis no attempt is made to identify quark flavours. However, the efficiency is found to be slightly higher for events containing b quarks than for events with light quarks. When $i = 3$, the decay products of the neutralino pair contain $\tau^+\tau^-$, $\tau\nu_\tau$ or $\nu_\tau\bar{\nu}_\tau$. Since taus are selected with lower efficiency with respect to electrons or muons, this choice of the first generation index provides a conservative estimate for the signal efficiency. The lowest selection efficiency is thus found for the choice $\lambda'_{ijk} = \lambda'_{311}$, that will be quoted in the following.

After the preselection is applied, 11099 events are selected in the data sample and 11022$\pm$34 events are expected from Standard Model processes, of which 7677 events are from $q\bar{q}$, 2481 from W^+W^- decays and 674 from hadronic two-photon interactions. Figure 2 shows the $\ln(y_{34})$, thrust, normalised visible energy and polar angle of the missing momentum distributions after the preselection. The data are in good agreement with the Monte Carlo expectations.

The five groups of final selections are shown in Tables 14 to 20 of Appendix A. The lowest selection efficiencies correspond to $\lambda'_{ijk} = \lambda'_{311}$, and are summarized in Tables 3 and 4.

In the case of neutralino and chargino direct decays the lowest selection efficiency is obtained in the intermediate mass region (for mass values around 50 GeV) where the W^+W^- background can not be efficiently rejected by a cut on the thrust.

For indirect chargino decays and for a chargino mass of 94 GeV the efficiencies decrease for high values of ΔM, since in this region the signal signatures are very similar to those of W pair-production.

In the case of dominant λ'_{ijk} couplings, scalar leptons can decay indirectly: $\tilde{\ell}_R \rightarrow \ell\,\tilde{\chi}^0_1 \rightarrow \ell\ell qq,\ \ell\nu qq$. The efficiencies for indirect decays are listed in Table 4. Only $\tilde{e}^+_R\tilde{e}^-_R$ production is considered. The efficiency is highest for large ΔM, when the two energetic electrons give a clear signature.

Supersymmetric partners of the right-handed leptons have no direct two-body decays via λ'_{ijk} couplings (Table 1). However, when scalar leptons are lighter than $\tilde{\chi}^0_1$, the four-body [3] decay $\tilde{\ell}_R \rightarrow \ell\ell qq$ or $\tilde{\ell}_R \rightarrow \ell\nu qq$ can occur. This leads to the same final states as those resulting from $\tilde{\ell}_R$ indirect decays, but with virtual $\tilde{\chi}^0_1$ production. Since non-resonant four-body decays are not implemented in the generator [12], we have used the results of the indirect decay analysis, with a procedure analogous to the one described at the end of Section 6.

6 $\boldsymbol{\lambda''_{ijk}}$ Analysis

Table 6 shows the topologies arising when the λ''_{ijk} couplings dominate. The flavour composition depends on the generation indices. In the case of neutralino and chargino pair-production, the different topologies can be classified into two groups: multijets and multijets with leptons and/or missing energy. After a common preselection, dedicated selections are developed for each group, depending on the particle boosts, the ΔM values and the virtual W decay products. The following process is also considered: $e^+e^- \rightarrow \tilde{\ell}^+_R\tilde{\ell}^-_R \rightarrow qqqqqq\ell^+\ell^-$, for which a third group of selections is performed, taking into account the lepton flavour.

The preselection of the λ''_{ijk} analysis aims at selecting well balanced hadronic events. Low multiplicity events, such as leptonic Z and W decays, are rejected by requiring at least 13 calorimetric clusters. At least one charged track has to be present. The visible energy has to be greater than 70% of $\sqrt{s}$. The energy imbalances, parallel (E_{par}) and perpendicular (E_{perp}) to the beam direction, are required to be less than 20% of the visible energy. Unbalanced events with an ISR photon in the beam pipe are removed by means of the requirement on the parallel energy imbalance. In order to reject events with an ISR photon seen in the detector, the invariant mass of the hadronic system ($\sqrt{s'}$) has to be greater than 80% of $\sqrt{s}$. In order to remove background contributions from two-photon interactions, the energy in a cone of 12° half-opening angle around the beam axis has not to exceed 30% of the total visible energy. Furthermore, the thrust axis is required to be well contained in the detector with a polar angle (θ_T) between 8° and 172°.

Also in this analysis no attempt is made to identify quark flavours. However, the efficiency is found to be slightly lower for events containing light quarks than for events with b quarks. Therefore, only the results obtained by the choice $\lambda''_{ijk} = \lambda''_{212}$ will be quoted in the next sections. After the preselection is applied, 5492 events are selected in the data sample and 5463 ± 32 are expected from Standard Model processes, of which 3803 are $q\bar{q}$ and 1431 are W^+W^- events. Figure 3 shows the $\ln(y_{34})$, thrust, $\ln(y_{45})$ and width of the most energetic jet

Direct decays		Selections
$e^+e^- \to \tilde{\chi}^0_m \tilde{\chi}^0_n \;\to$	qqqqqq	multijets
$e^+e^- \to \tilde{\chi}^+_1 \tilde{\chi}^-_1 \;\to$	qqqqqq	multijets
Indirect decays		
$e^+e^- \to \tilde{\chi}^0_m \tilde{\chi}^0_{n(n\geq 2)} \to$	qqqqqq qq qqqqqq $\ell\ell$ qqqqqq $\nu\nu$	multijets multijets + lepton(s) multijets
$e^+e^- \to \tilde{\chi}^+_1 \tilde{\chi}^-_1 \;\to$	qqqqqq qqqq qqqqqq qq $\ell\nu$ qqqqqq $\ell\ell\nu\nu$	multijets multijets + lepton(s) multijets + lepton(s)
$e^+e^- \to \tilde{\ell}^+_R \tilde{\ell}^-_R \;\to$	qqqqqq $\ell\ell$	6 jets + 2 ℓ

Table 6: Processes considered in the λ''_{ijk} coupling analysis and corresponding selections. For masses below 50 GeV or small ΔM values not all jets in the event can be resolved. $\tilde{\chi}^0_m \tilde{\chi}^0_n$ indicates neutralino pair-production with $m = 1, 2$ and $n = 1, .., 4$. For final states with neutrinos we use selections with no explicit missing energy requirement, because for those topologies $\not{E}$ is small.

(W_{jet1}) distributions after the preselection. The width of a jet is defined as p_T^{jet}/E^{jet}, where the event is clustered into exactly two jets, ordered with decreasing energies, and p_T^{jet} is the sum of the projections of the particle momenta on to a plane perpendicular to the jet axis. There is good agreement between data and Monte Carlo expectations.

The three groups of final selections are shown in Tables 21 to 23 of Appendix A. The efficiencies are summarized in Tables 3 and 4.

For direct neutralino and chargino decays, the efficiencies increase with increasing mass of the supersymmetric particle. At high masses, the six quarks are expected to be isotropically produced, while for low mass values signal events are produced back-to-back and are selected with lower efficiencies due to cuts required to reduce the dominant background coming from the two-fermion processes.

In the case of indirect decays and for a chargino mass of 94 GeV the efficiencies slightly decrease at high values of ΔM, where the signal signatures are very similar to those of W^+W^- background. Leptons and neutrinos from virtual W decays can carry a large fraction of the event energy when ΔM is large, leading to lower selection efficiencies.

For $M_{\tilde{\chi}^0_m} + M_{\tilde{\chi}^0_n} = 188$ GeV, the efficiencies of the process $e^+e^- \to \tilde{\chi}^0_m \tilde{\chi}^0_n$ $(m = 1, 2, n = 2, 3, 4)$ decrease slightly with increasing ΔM.

Scalar leptons can decay indirectly: $\tilde{\ell}_R \to \ell\, \tilde{\chi}^0_1 \to \ell$qqq. The efficiencies for these indirect decays are also listed in Table 4.

For scalar electron and scalar muon decays, the efficiencies are highest for medium $\Delta M = M_{\tilde{\ell}_R} - M_{\tilde{\chi}^0_1}$ values, where events have a high multiplicity satisfying the multijet selections and two energetic leptons which are well identified.

Supersymmetric partners of the right-handed leptons have no direct two-body decays via λ''_{ijk} couplings (Table 1). However, when scalar leptons are lighter than $\tilde{\chi}^0_1$, the four-body [3] decay $\tilde{\ell}_R \to \ell$qqq can occur and this provides the same final state ℓqqq as that resulting from indirect decays, but with virtual $\tilde{\chi}^0_1$ production.

The non-resonant four-body decay is not implemented in the generator, which allows only scalar lepton decays via on-shell neutralino production. For this reason, we use the results of the indirect decay analysis, performing a scan over all neutralino mass values between 0 and $M_{\tilde{\ell}_R}$, for each value of $M_{\tilde{\ell}_R}$. The resulting lowest efficiency is conservatively quoted in the following for four-body decays. It is found in most cases for $M_{\tilde{\chi}^0_1} \simeq M_{\tilde{\ell}_R}$, that the resulting low energy lepton can not be separated from a nearby jet. For scalar taus with masses above 70 GeV the lowest efficiency is found for high ΔM values, as in the case of indirect decays.

7 Model Independent Results

Table 7 and Table 8 show the number of candidates and expected background events for the different selections and processes, respectively. The same process may give rise to different final states (such as chargino direct decays via λ_{ijk}) or the same final state (like "multijets") can be present as a decay product of more than one process.

No excess of events is observed. Therefore upper limits are set on the neutralino, chargino and scalar lepton production cross sections assuming direct or indirect R-parity violating decays. Figure 4 shows the 95% confidence level (C.L.) upper limits on neutralino and chargino pair-production cross sections. The 95% C.L. upper limits on scalar lepton pair-production cross sections are shown in Figures 5 and 6. These limits are derived by taking into account the estimated background contamination. Systematic uncertainties on the signal efficiency are dominated by Monte Carlo statistics. The typical relative error is 5% and it is taken into account in the calculations of the signal upper limits [24].

8 Interpretation in the MSSM

The results are also interpreted as excluded regions in the MSSM parameter space. In the MSSM framework, neutralino and chargino masses, couplings and cross sections depend on the gaugino mass parameter, M_2, the higgsino mass mixing parameter, μ, the ratio of the vacuum expectation values of the two Higgs doublets, $\tan\beta$, and the common mass of the scalar particles at the GUT scale, m_0. Therefore the excluded regions in the (M_2, μ) plane are a function of the values of m_0 and $\tan\beta$. The results presented in this section are obtained performing a scan over $0 \leq M_2 \leq 1000$ GeV, -500 GeV $\leq \mu \leq 500$ GeV, $0 \leq m_0 \leq 500$ GeV and $0.7 \leq \tan\beta \leq 40$. They do not depend on the value of the trilinear coupling in the Higgs sector, A.

A point in the MSSM parameter space is excluded if the total number of expected events is greater than the combined upper limit at 95% C.L. on the number of signal events. Neutralino, chargino and scalar lepton analyses are combined since several processes can occur at a given point.

In addition to the limits obtained with this analysis, we take into account the constraints from the L3 cross section measurements at the Z pole. A point in the MSSM parameter space is excluded at 95% C.L. by Z lineshape measurements if:

$$(\frac{\sigma_{SUSY}}{\sigma_{\mathrm{Z}}})\,\Gamma_{\mathrm{Z}} > \Gamma_{LIM}\,, \tag{3}$$

where σ_{SUSY} is the sum of the pair-production cross sections of supersymmetric particles at the Z pole, calculated with `SUSYGEN`. σ_{Z} is the measured total Z cross section, Γ_{Z} and $\Gamma_{LIM} =$ 22 MeV are the measured total Z width and the 95% C.L. upper limit on possible non-Standard Model contributions to the total Z width [23].

Coupling	Selection	N_{back}	N_{data}
λ_{ijk}	$4\ell + \not{E}$	2.0 ± 0.2	3
	$(\geq 4)\,\ell +$ (jets) $+\not{E}$	3.8 ± 0.3	2
	$2\ell + \not{E}$	18 ± 1	18
	6ℓ	0.26 ± 0.05	0
λ'_{ijk}	4 jets $+ 2\tau$	30.0 ± 0.7	26
	4 jets $+ \not{E}$	28.9 ± 0.8	31
	4 jets $+ \tau + \not{E}$	29.4 ± 1.2	25
	Multijets + lepton(s)	6.1 ± 0.2	8
	Multijets $+ \not{E}$	65 ± 1	68
	Multijets + lepton(s) $+ \not{E}$	11.7 ± 0.2	10
	Multijets	194 ± 1	187
	Scalar leptons	26.4 ± 0.6	27
λ''_{ijk}	Multijets ($M_{\tilde{\chi}^0_1} =$ 20–30 GeV)	47 ± 1	42
	Multijets ($M_{\tilde{\chi}^0_1} =$ 30–40 GeV)	79 ± 1	81
	Multijets ($M_{\tilde{\chi}^0_1} =$ 40–50 GeV)	48.1 ± 0.9	47
	Multijets ($M_{\tilde{\chi}^0_1} =$ 50–60 GeV)	98 ± 1	100
	Multijets	194 ± 1	187
	Multijets + lepton(s) (Semileptonic)	1.6 ± 0.2	3
	Multijets + lepton(s) (Leptonic)	3.2 ± 0.1	3
	Scalar leptons	154 ± 1	157

Table 7: Number of observed data (N_{data}) and expected background (N_{back}) events for the different selections. A process can give rise to several topologies, or the same topology may occur in more than one final state. The error on the expected background is due to Monte Carlo statistics.

Coupling	Process	N_{back}	N_{data}
λ_{ijk}	$\tilde{\chi}^0_1\tilde{\chi}^0_1$	2.0 ± 0.2	3
	$\tilde{\chi}^0_m\tilde{\chi}^0_n$	5.8 ± 0.4	5
	$\tilde{\chi}^+_1\tilde{\chi}^-_1$ (indirect)	3.8 ± 0.3	2
	$\tilde{\chi}^+_1\tilde{\chi}^-_1$ (direct)	20 ± 1	21
	$\tilde{\ell}^+_R\tilde{\ell}^-_R$ (direct)	18 ± 1	18
	$\tilde{\nu}\tilde{\nu}$	5.8 ± 0.4	5
λ'_{ijk}	$\tilde{\chi}^0_1\tilde{\chi}^0_1$	77 ± 2	70
	$\tilde{\chi}^+_1\tilde{\chi}^-_1$	262 ± 2	257
	$\tilde{e}^+_R\tilde{e}^-_R$	26.4 ± 0.6	27
λ''_{ijk}	$\tilde{\chi}^0_1\tilde{\chi}^0_1$	357 ± 3	353
	$\tilde{\chi}^+_1\tilde{\chi}^-_1$	197 ± 1	193
	$\tilde{\ell}^+_R\tilde{\ell}^-_R$	154 ± 1	157

Table 8: Number of observed data (N_{data}) and expected background (N_{back}) events for the different processes. Details on the selection of each topology are given in Table 7. The error on the expected background is due to Monte Carlo statistics.

Figures 7 and 8 show the excluded regions at 95% C.L. in the (M_2, μ) plane for $\tan\beta = \sqrt{2}$ and $m_0 = 500$ GeV, and for $\tan\beta = 40$ and $m_0 = 70$ GeV. Some regions beyond the chargino kinematic limit are excluded at large m_0 and low $\tan\beta$ values by the $\tilde{\chi}^0_m\tilde{\chi}^0_{n(n\geq2)}$ analyses (Figure 7) and at low m_0 by the $\tilde{\chi}^0_1\tilde{\chi}^0_1$ analyses (Figure 8).

8.1 Lightest scalar lepton $\tilde{\ell}_R$ as LSP

For $0 \leq m_0 < 50$ GeV and $1 \leq \tan\beta < 2$ the lightest scalar lepton, the supersymmetric partner of the right-handed electron, can be the LSP. In this region, in the presence of dominant λ_{ijk} coupling, the decay chain $\tilde{\chi}^0_1 \rightarrow \ell\tilde{\ell}_R \rightarrow \ell\ell\nu$ leads to the same final states as those arising from neutralino direct R-parity violating decays, so that the analysis is efficient also when the lightest scalar lepton is the LSP.

When the λ'_{ijk} or λ''_{ijk} couplings dominate, the decays $\tilde{\chi}^0_1 \rightarrow \ell\tilde{\ell}_R \rightarrow \ell\ell\ell(\nu)$qq or $\tilde{\chi}^0_1 \rightarrow \ell\tilde{\ell}_R \rightarrow \ell\ell$qqq occur, respectively. Those five-body decays are not implemented in `SUSYGEN`. However, since in this region $\tilde{\ell}_R$ is lighter than $\tilde{\chi}^0_1$, we can take into account the scalar lepton decays $\tilde{\ell}_R \rightarrow \ell\ell(\nu)$qq or $\tilde{\ell}_R \rightarrow \ell$qqq, as described at the end of Sections 5 and 6.

8.2 Mass Limits

Figure 9 shows the 95% C.L. lower limits on neutralino and scalar lepton masses as a function of $\tan\beta$. The $\tilde{\chi}^0_1$ and $\tilde{\chi}^0_2$ mass limits are shown for $m_0 = 500$ GeV and the $\tilde{\ell}_R$ ones for $m_0 = 0$. At low m_0 ($m_0 \leq 70$ GeV), neutralino and scalar lepton pair-production is enhanced, allowing to obtain better results also at low values of $\tan\beta$. For high m_0 values, these contributions are suppressed and the mass limit is given by the chargino exclusion. The absolute minimum on the scalar lepton mass is found at $m_0 = 0$. For low m_0 values the different contributions depend on $\tan\beta$, since the $\tilde{\ell}_R$ can be the LSP for low $\tan\beta$ values ($\tan\beta < 2$) and therefore only the scalar lepton analysis contributes to the limit in this region. For higher values of $\tan\beta$, $\tilde{\chi}^0_1$ is the LSP, and the lower limit on the scalar lepton mass is mainly given by the $\tilde{\chi}^0_1\tilde{\chi}^0_1$ exclusion contours. As an example, Figure 10a and 10b show the 95% C.L. lower limits on the mass of the supersymmetric partner of the right-handed electron for $\tan\beta = 1$ and 2, respectively.

The minima on the 95% C.L. lower mass limits shown in Figure 9 correspond to the absolute minima from the complete scan on M_2, μ, m_0 and $\tan\beta$. The absolute limit on $M_{\tilde{\ell}_R}$ is found at $\tan\beta = 0.7$ in the case of λ_{ijk} and λ'_{ijk} and at $\tan\beta = 1.4$ for λ''_{ijk}. The difference is due to the lower cross-section upper limit of λ''_{ijk} for scalar lepton direct decays (Figure 5), since for λ_{ijk} and λ'_{ijk} the limit on $M_{\tilde{\ell}_R}$ is found when the $\tilde{\ell}_R$ is the LSP. Figure 11 shows similar mass limits for $m_0 = 50$ GeV. The chargino mass limit is almost independent of $\tan\beta$, being close to the kinematic limit for any value of $\tan\beta$ and m_0.

We derive lower limits at 95% C.L. on the neutralino, chargino and scalar lepton masses, as detailed in Table 9. All analysis contributions (neutralino, chargino and scalar lepton searches) are taken into account simultaneously under the assumption of gaugino and scalar masses unification at the GUT scale.

Identical scalar lepton mass limits are obtained even without the assumption of common scalar masses at the GUT scale. For λ_{ijk} and λ'_{ijk} the present bounds on the scalar lepton masses are found in the case in which the $\tilde{\ell}_R$ is the LSP. For λ''_{ijk} this happens when the $\tilde{\ell}_R$ and $\tilde{\chi}^0_1$ are nearly degenerate in mass. In both cases the neutralino analyses give the main contribution to the exclusion in the regions of the parameter space around the limit. The remaining sensitivity is due to searches for direct slepton decays via λ_{ijk}. As these searches are equally sensitive to scalar electron, muon or tau signals as shown in Figure 5, the limits are unchanged.

Particle Mass	λ_{ijk}	λ'_{ijk}	λ''_{ijk}
$M_{\tilde{\chi}^0_1}$	32.6 GeV	32.5 GeV	32.5 GeV
$M_{\tilde{\chi}^0_2}$	69.5 GeV	68.0 GeV	68.0 GeV
$M_{\tilde{\chi}^0_3}$	99.3 GeV	99.0 GeV	99.0 GeV
$M_{\tilde{\chi}^\pm_1}$	94.3 GeV	93.8 GeV	93.8 GeV
$M_{\tilde{\ell}_R}$	75.9 GeV	68.8 GeV	77.5 GeV
$M_{\tilde{\nu}}$	141.2 GeV	–	–

Table 9: Lower limits at 95% C.L. on the masses of the supersymmetric particles considered in this analysis. The limits on $M_{\tilde{\ell}_R}$ hold for $\tilde{\mathrm{e}}_R$, $\tilde{\mu}_R$ and $\tilde{\tau}_R$.

The search for R-parity violating decays of supersymmetric particles reaches at least the same sensitivity as in the R-parity conserving case [6]. Therefore, the supersymmetry limits obtained at LEP are independent of R-parity conservation assumptions.

Acknowledgements

We wish to express our gratitude to the CERN accelerator divisions for the excellent performance of the LEP machine. We acknowledge the contributions of the engineers and technicians who have participated in the construction and maintenance of this experiment.

References

[1] A review can be found for example in:
H.E. Haber and G.L. Kane, Phys. Rep. **117** (1985) 75.

[2] C.S. Aulakh and R.N. Mohapatra, Phys. Lett. **B 119** (1982) 136;
F. Zwirner, Phys. Lett. **B 132** (1983) 103;
L.J. Hall and M. Suzuki, Nucl. Phys. **B 231** (1984) 419.
For a recent review and a reference to the literature:
H. Dreiner, "An introduction to explicit R-parity violation", hep–ph/9707435, published in *Perspectives on Supersymmetry*, ed. G.L. Kane, World Scientific, Singapore (1998).

[3] R. Barbieri and A. Masiero, Nucl. Phys. **B 267** (1986) 679.

[4] S. Weinberg, Phys. Rev. **D 26** (1982) 287;
G. Bhattacharyya and P.B. Pal, hep–ph/9809493, Phys. Rev. **D 59** (1999) 097701.

[5] Particle Data Group, D.E. Groom *et al.*, Eur. Phys. J. **C 15** (2000) 1.

[6] L3 Collab., M. Acciarri *et al.*, Phys. Lett. **B 471** (1999) 280, Phys. Lett. **B 472** (2000) 420 and references therein.

[7] L3 Collab., M. Acciarri *et al.*, Phys. Lett. **B 489** (2000) 81.

[8] S. Dawson, Nucl. Phys. **B 261** (1985) 297.

[9] L3 Collab., M. Acciarri *et al.*, Phys. Lett. **B 459** (1999) 354.

[10] ALEPH Collab., D. Buskulic *et al.*, Phys. Lett. **B 349** (1995) 238;
ALEPH Collab., D. Buskulic *et al.*, Phys. Lett. **B 384** (1996) 461;
ALEPH Collab., R. Barate *et al.*, Eur. Phys. J. **C 4** (1998) 433;
ALEPH Collab., R. Barate *et al.*, Eur. Phys. J. **C 7** (1999) 383;
ALEPH Collab., R. Barate *et al.*, Eur. Phys. J. **C 13** (2000) 29;
DELPHI Collab., P. Abreu *et al.*, Eur. Phys. J. **C 13** (2000) 591;
DELPHI Collab., P. Abreu *et al.*, Phys. Lett. **B 487** (2000) 36;
OPAL Collab., G. Abbiendi *et al.*, Eur. Phys. J. **C 11** (1999) 619;
OPAL Collab., G. Abbiendi *et al.*, Eur. Phys. J. **C 12** (2000) 1.

[11] L3 Collab., B. Adeva *et al.*, Nucl. Instr. and Meth. **A 289** (1990) 35;
J.A. Bakken *et al.*, Nucl. Instr. and Meth. **A 275** (1989) 81;
O. Adriani *et al.*, Nucl. Instr. and Meth. **A 302** (1991) 53;
B. Adeva *et al.*, Nucl. Instr. and Meth. **A 323** (1992) 109;
K. Deiters *et al.*, Nucl. Instr. and Meth. **A 323** (1992) 162;
M. Chemarin *et al.*, Nucl. Instr. and Meth. **A 349** (1994) 345;
M. Acciarri *et al.*, Nucl. Instr. and Meth. **A 351** (1994) 300;
G. Basti *et al.*, Nucl. Instr. and Meth. **A 374** (1996) 293;
I.C. Brock *et al.*, Nucl. Instr. and Meth. **A 381** (1996) 236;
A. Adam *et al.*, Nucl. Instr. and Meth. **A 383** (1996) 342.

[12] S. Katsanevas and S. Melachroinos, Proceedings of the Workshop "Physics at LEP 2", eds. G. Altarelli, T. Sjöstrand and F. Zwirner, CERN 96-01 (1996), vol. 2, p. 328.
`SUSYGEN 2.2`, S. Katsanevas and P. Morawitz, Comp. Phys. Comm. **112** (1998) 227.

[13] `PYTHIA` Version 5.722 is used.
T. Sjöstrand, preprint CERN-TH/7112/93 (1993), revised August 1995; Comp. Phys. Comm. **82** (1994) 74, hep-ph/0001032.

[14] S. Jadach *et al.*, Phys. Lett. **B 390** (1997) 298.

[15] `KORALZ` Version 4.02 is used.
S. Jadach, B.F.L. Ward, and Z. Wąs, Comp. Phys. Comm. **79** (1994) 503.

[16] `PHOJET` Version 1.05 is used.
R. Engel, Z. Phys. **C 66** (1995) 203;
R. Engel and J. Ranft, Phys. Rev. **D 54** (1996) 4244.

[17] F.A. Berends, P.H. Daverveldt and R. Kleiss, Nucl. Phys. **B 253** (1985) 441.

[18] `KORALW` Version 1.33 is used.
M. Skrzypek *et al.*, Comp. Phys. Comm. **94** (1996) 216;
M. Skrzypek *et al.*, Phys. Lett. **B 372** (1996) 289.

[19] F.A. Berends, R. Kleiss and R. Pittau, Comp. Phys. Comm. **85** (1995) 437.

[20] `GEANT` Version 3.15 is used.
R. Brun *et al.*, preprint CERN DD/EE/84-1 (Revised 1987).

[21] H. Fesefeldt, RWTH Aachen Report PITHA 85/2 (1985).

[22] S. Catani *et al.*, Phys. Lett. **B 269** (1991) 432;
S. Bethke *et al.*, Nucl. Phys. **B 370** (1992) 310;
N. Brown and W.J. Stirling, Z. Phys. **C 53** (1992) 629.

[23] L3 Collab., M. Acciarri *et al.*, Eur. Phys. J. **C 16** (2000) 1.

[24] R.D. Cousins and V.L. Highland, Nucl. Instr. and. Meth. **A 320** (1992) 331.

[25] J.F. Grivaz and F. Le Diberder, preprint LAL 92-37 (1992).

The L3 Collaboration:

M.Acciarri,[26] P.Achard,[19] O.Adriani,[16] M.Aguilar-Benitez,[25] J.Alcaraz,[25] G.Alemanni,[22] J.Allaby,[17] A.Aloisio,[28] M.G.Alviggi,[28] G.Ambrosi,[19] H.Anderhub,[48] V.P.Andreev,[6,36] T.Angelescu,[12] F.Anselmo,[9] A.Arefiev,[27] T.Azemoon,[3] T.Aziz,[10] P.Bagnaia,[35] A.Bajo,[25] L.Baksay,[43] A.Balandras,[4] S.V.Baldew,[2] S.Banerjee,[10] Sw.Banerjee,[10] A.Barczyk,[48,46] R.Barillère,[17] P.Bartalini,[22] M.Basile,[9] N.Batalova,[45] R.Battiston,[32] A.Bay,[22] F.Becattini,[16] U.Becker,[14] F.Behner,[48] L.Bellucci,[16] R.Berbeco,[3] J.Berdugo,[25] P.Berges,[14] B.Bertucci,[32] B.L.Betev,[48] S.Bhattacharya,[10] M.Biasini,[32] A.Biland,[48] J.J.Blaising,[4] S.C.Blyth,[33] G.J.Bobbink,[2] A.Böhm,[1] L.Boldizsar,[13] B.Borgia,[35] D.Bourilkov,[48] M.Bourquin,[19] S.Braccini,[19] J.G.Branson,[39] F.Brochu,[4] A.Buffini,[16] A.Buijs,[44] J.D.Burger,[14] W.J.Burger,[32] X.D.Cai,[14] M.Capell,[14] G.Cara Romeo,[9] G.Carlino,[28] A.M.Cartacci,[16] J.Casaus,[25] G.Castellini,[16] F.Cavallari,[35] N.Cavallo,[37] C.Cecchi,[32] M.Cerrada,[25] F.Cesaroni,[23] M.Chamizo,[19] Y.H.Chang,[50] U.K.Chaturvedi,[18] M.Chemarin,[24] A.Chen,[50] G.Chen,[7] G.M.Chen,[7] H.F.Chen,[20] H.S.Chen,[7] G.Chiefari,[28] L.Cifarelli,[38] F.Cindolo,[9] C.Civinini,[16] I.Clare,[14] R.Clare,[14] G.Coignet,[4] N.Colino,[25] S.Costantini,[5] F.Cotorobai,[12] B.de la Cruz,[25] A.Csilling,[13] S.Cucciarelli,[32] T.S.Dai,[14] J.A.van Dalen,[30] R.D'Alessandro,[16] R.de Asmundis,[28] P.Déglon,[19] A.Degré,[4] K.Deiters,[46] D.della Volpe,[28] E.Delmeire,[19] P.Denes,[34] F.DeNotaristefani,[35] A.De Salvo,[48] M.Diemoz,[35] M.Dierckxsens,[2] D.van Dierendonck,[2] C.Dionisi,[35] M.Dittmar,[48] A.Dominguez,[39] A.Doria,[28] M.T.Dova,[18,♯] D.Duchesneau,[4] D.Dufournaud,[4] P.Duinker,[2] I.Duran,[40] H.El Mamouni,[24] A.Engler,[33] F.J.Eppling,[14] F.C.Erné,[2] P.Extermann,[19] M.Fabre,[46] M.A.Falagan,[25] S.Falciano,[35,17] A.Favara,[17] J.Fay,[24] O.Fedin,[36] M.Felcini,[48] T.Ferguson,[33] H.Fesefeldt,[1] E.Fiandrini,[32] J.H.Field,[19] F.Filthaut,[17] P.H.Fisher,[14] I.Fisk,[39] G.Forconi,[14] K.Freudenreich,[48] C.Furetta,[26] Yu.Galaktionov,[27,14] S.N.Ganguli,[10] P.Garcia-Abia,[5] M.Gataullin,[31] S.S.Gau,[11] S.Gentile,[35,17] N.Gheordanescu,[12] S.Giagu,[35] Z.F.Gong,[20] G.Grenier,[24] O.Grimm,[48] M.W.Gruenewald,[8] M.Guida,[38] R.van Gulik,[2] V.K.Gupta,[34] A.Gurtu,[10] L.J.Gutay,[45] D.Haas,[5] A.Hasan,[29] D.Hatzifotiadou,[9] T.Hebbeker,[8] A.Hervé,[17] P.Hidas,[13] J.Hirschfelder,[33] H.Hofer,[48] G. Holzner,[48] H.Hoorani,[33] S.R.Hou,[50] Y.Hu,[30] I.Iashvili,[47] B.N.Jin,[7] L.W.Jones,[3] P.de Jong,[2] I.Josa-Mutuberría,[25] R.A.Khan,[18] M.Kaur,[18,◇] M.N.Kienzle-Focacci,[19] D.Kim,[35] J.K.Kim,[42] J.Kirkby,[17] D.Kiss,[13] W.Kittel,[30] A.Klimentov,[14,27] A.C.König,[30] M.Kopal,[45] A.Kopp,[47] V.Koutsenko,[14,27] M.Kräber,[48] R.W.Kraemer,[33] W.Krenz,[1] A.Krüger,[47] A.Kunin,[14,27] P.Ladron de Guevara,[25] I.Laktineh,[24] G.Landi,[16] M.Lebeau,[17] A.Lebedev,[14] P.Lebrun,[24] P.Lecomte,[48] P.Lecoq,[17] P.Le Coultre,[48] H.J.Lee,[8] J.M.Le Goff,[17] R.Leiste,[47] P.Levtchenko,[36] C.Li,[20] S.Likhoded,[47] C.H.Lin,[50] W.T.Lin,[50] F.L.Linde,[2] L.Lista,[28] Z.A.Liu,[7] W.Lohmann,[47] E.Longo,[35] Y.S.Lu,[7] K.Lübelsmeyer,[1] C.Luci,[17,35] D.Luckey,[14] L.Lugnier,[24] L.Luminari,[35] W.Lustermann,[48] W.G.Ma,[20] M.Maity,[10] L.Malgeri,[17] A.Malinin,[17] C.Maña,[25] D.Mangeol,[30] J.Mans,[34] G.Marian,[15] J.P.Martin,[24] F.Marzano,[35] K.Mazumdar,[10] R.R.McNeil,[6] S.Mele,[17] L.Merola,[28] M.Meschini,[16] W.J.Metzger,[30] M.von der Mey,[1] A.Mihul,[12] H.Milcent,[17] G.Mirabelli,[35] J.Mnich,[1] G.B.Mohanty,[10] T.Moulik,[10] G.S.Muanza,[24] A.J.M.Muijs,[2] B.Musicar,[39] M.Musy,[35] M.Napolitano,[28] F.Nessi-Tedaldi,[48] H.Newman,[31] T.Niessen,[1] A.Nisati,[35] H.Nowak,[47] R.Ofierzynski,[48] G.Organtini,[35] A.Oulianov,[27] C.Palomares,[25] D.Pandoulas,[1] S.Paoletti,[35,17] P.Paolucci,[28] R.Paramatti,[35] H.K.Park,[33] I.H.Park,[42] G.Passaleva,[17] S.Patricelli,[28] T.Paul,[11] M.Pauluzzi,[32] C.Paus,[17] F.Pauss,[48] M.Pedace,[35] S.Pensotti,[26] D.Perret-Gallix,[4] B.Petersen,[30] D.Piccolo,[28] F.Pierella,[9] M.Pieri,[16] P.A.Piroué,[34] E.Pistolesi,[26] V.Plyaskin,[27] M.Pohl,[19] V.Pojidaev,[27,16] H.Postema,[14] J.Pothier,[17] D.O.Prokofiev,[45] D.Prokofiev,[36] J.Quartieri,[38] G.Rahal-Callot,[48,17] M.A.Rahaman,[10] P.Raics,[15] N.Raja,[10] R.Ramelli,[48] P.G.Rancoita,[26] R.Ranieri,[16] A.Raspereza,[47] G.Raven,[39] P.Razis,[29] D.Ren,[48] M.Rescigno,[35] S.Reucroft,[11] S.Riemann,[47] K.Riles,[3] J.Rodin,[43] B.P.Roe,[3] L.Romero,[25] A.Rosca,[8] S.Rosier-Lees,[4] J.A.Rubio,[17] G.Ruggiero,[16] H.Rykaczewski,[48] S.Saremi,[6] S.Sarkar,[35] J.Salicio,[17] E.Sanchez,[17] M.P.Sanders,[30] C.Schäfer,[17] V.Schegelsky,[36] S.Schmidt-Kaerst,[1] D.Schmitz,[1] H.Schopper,[49] D.J.Schotanus,[30] G.Schwering,[1] C.Sciacca,[28] A.Seganti,[9] L.Servoli,[32] S.Shevchenko,[31] N.Shivarov,[41] V.Shoutko,[27] E.Shumilov,[27] A.Shvorob,[31] T.Siedenburg,[1] D.Son,[42] B.Smith,[33] P.Spillantini,[16] M.Steuer,[14] D.P.Stickland,[34] A.Stone,[6] B.Stoyanov,[41] A.Straessner,[1] K.Sudhakar,[10] G.Sultanov,[18] L.Z.Sun,[20] S.Sushkov,[8] H.Suter,[48] J.D.Swain,[18] Z.Szillasi,[43,¶] T.Sztaricskai,[43,¶] X.W.Tang,[7] L.Tauscher,[5] L.Taylor,[11] B.Tellili,[24] C.Timmermans,[30] Samuel C.C.Ting,[14] S.M.Ting,[14] S.C.Tonwar,[10] J.Tóth,[13] C.Tully,[17] K.L.Tung,[7] Y.Uchida,[14] J.Ulbricht,[48] E.Valente,[35] G.Vesztergombi,[13] I.Vetlitsky,[27] D.Vicinanza,[38] G.Viertel,[48] S.Villa,[11] M.Vivargent,[4] S.Vlachos,[5] I.Vodopianov,[36] H.Vogel,[33] H.Vogt,[47] I.Vorobiev,[33] A.A.Vorobyov,[36] A.Vorvolakos,[29] M.Wadhwa,[5] W.Wallraff,[1] M.Wang,[14] X.L.Wang,[20] Z.M.Wang,[20] A.Weber,[1] M.Weber,[1] P.Wienemann,[1] H.Wilkens,[30] S.X.Wu,[14] S.Wynhoff,[17] L.Xia,[31] Z.Z.Xu,[20] J.Yamamoto,[3] B.Z.Yang,[20] C.G.Yang,[7] H.J.Yang,[7] M.Yang,[7] J.B.Ye,[20] S.C.Yeh,[51] An.Zalite,[36] Yu.Zalite,[36] Z.P.Zhang,[20] G.Y.Zhu,[7] R.Y.Zhu,[31] A.Zichichi,[9,17,18] G.Zilizi,[43,¶] B.Zimmermann,[48] M.Zöller.[1]

1 I. Physikalisches Institut, RWTH, D-52056 Aachen, FRG[§]
III. Physikalisches Institut, RWTH, D-52056 Aachen, FRG[§]
2 National Institute for High Energy Physics, NIKHEF, and University of Amsterdam, NL-1009 DB Amsterdam, The Netherlands
3 University of Michigan, Ann Arbor, MI 48109, USA
4 Laboratoire d'Annecy-le-Vieux de Physique des Particules, LAPP,IN2P3-CNRS, BP 110, F-74941 Annecy-le-Vieux CEDEX, France
5 Institute of Physics, University of Basel, CH-4056 Basel, Switzerland
6 Louisiana State University, Baton Rouge, LA 70803, USA
7 Institute of High Energy Physics, IHEP, 100039 Beijing, China[△]
8 Humboldt University, D-10099 Berlin, FRG[§]
9 University of Bologna and INFN-Sezione di Bologna, I-40126 Bologna, Italy
10 Tata Institute of Fundamental Research, Bombay 400 005, India
11 Northeastern University, Boston, MA 02115, USA
12 Institute of Atomic Physics and University of Bucharest, R-76900 Bucharest, Romania
13 Central Research Institute for Physics of the Hungarian Academy of Sciences, H-1525 Budapest 114, Hungary[‡]
14 Massachusetts Institute of Technology, Cambridge, MA 02139, USA
15 KLTE-ATOMKI, H-4010 Debrecen, Hungary[¶]
16 INFN Sezione di Firenze and University of Florence, I-50125 Florence, Italy
17 European Laboratory for Particle Physics, CERN, CH-1211 Geneva 23, Switzerland
18 World Laboratory, FBLJA Project, CH-1211 Geneva 23, Switzerland
19 University of Geneva, CH-1211 Geneva 4, Switzerland
20 Chinese University of Science and Technology, USTC, Hefei, Anhui 230 029, China[△]
22 University of Lausanne, CH-1015 Lausanne, Switzerland
23 INFN-Sezione di Lecce and Università Degli Studi di Lecce, I-73100 Lecce, Italy
24 Institut de Physique Nucléaire de Lyon, IN2P3-CNRS,Université Claude Bernard, F-69622 Villeurbanne, France
25 Centro de Investigaciones Energéticas, Medioambientales y Tecnologícas, CIEMAT, E-28040 Madrid, Spain♭
26 INFN-Sezione di Milano, I-20133 Milan, Italy
27 Institute of Theoretical and Experimental Physics, ITEP, Moscow, Russia
28 INFN-Sezione di Napoli and University of Naples, I-80125 Naples, Italy
29 Department of Natural Sciences, University of Cyprus, Nicosia, Cyprus
30 University of Nijmegen and NIKHEF, NL-6525 ED Nijmegen, The Netherlands
31 California Institute of Technology, Pasadena, CA 91125, USA
32 INFN-Sezione di Perugia and Università Degli Studi di Perugia, I-06100 Perugia, Italy
33 Carnegie Mellon University, Pittsburgh, PA 15213, USA
34 Princeton University, Princeton, NJ 08544, USA
35 INFN-Sezione di Roma and University of Rome, "La Sapienza", I-00185 Rome, Italy
36 Nuclear Physics Institute, St. Petersburg, Russia
37 INFN-Sezione di Napoli and University of Potenza, I-85100 Potenza, Italy
38 University and INFN, Salerno, I-84100 Salerno, Italy
39 University of California, San Diego, CA 92093, USA
40 Dept. de Fisica de Particulas Elementales, Univ. de Santiago, E-15706 Santiago de Compostela, Spain
41 Bulgarian Academy of Sciences, Central Lab. of Mechatronics and Instrumentation, BU-1113 Sofia, Bulgaria
42 Laboratory of High Energy Physics, Kyungpook National University, 702-701 Taegu, Republic of Korea
43 University of Alabama, Tuscaloosa, AL 35486, USA
44 Utrecht University and NIKHEF, NL-3584 CB Utrecht, The Netherlands
45 Purdue University, West Lafayette, IN 47907, USA
46 Paul Scherrer Institut, PSI, CH-5232 Villigen, Switzerland
47 DESY, D-15738 Zeuthen, FRG
48 Eidgenössische Technische Hochschule, ETH Zürich, CH-8093 Zürich, Switzerland
49 University of Hamburg, D-22761 Hamburg, FRG
50 National Central University, Chung-Li, Taiwan, China
51 Department of Physics, National Tsing Hua University, Taiwan, China
§ Supported by the German Bundesministerium für Bildung, Wissenschaft, Forschung und Technologie
‡ Supported by the Hungarian OTKA fund under contract numbers T019181, F023259 and T024011.
¶ Also supported by the Hungarian OTKA fund under contract numbers T22238 and T026178.
♭ Supported also by the Comisión Interministerial de Ciencia y Tecnología.
♯ Also supported by CONICET and Universidad Nacional de La Plata, CC 67, 1900 La Plata, Argentina.
◇ Also supported by Panjab University, Chandigarh-160014, India.
△ Supported by the National Natural Science Foundation of China.

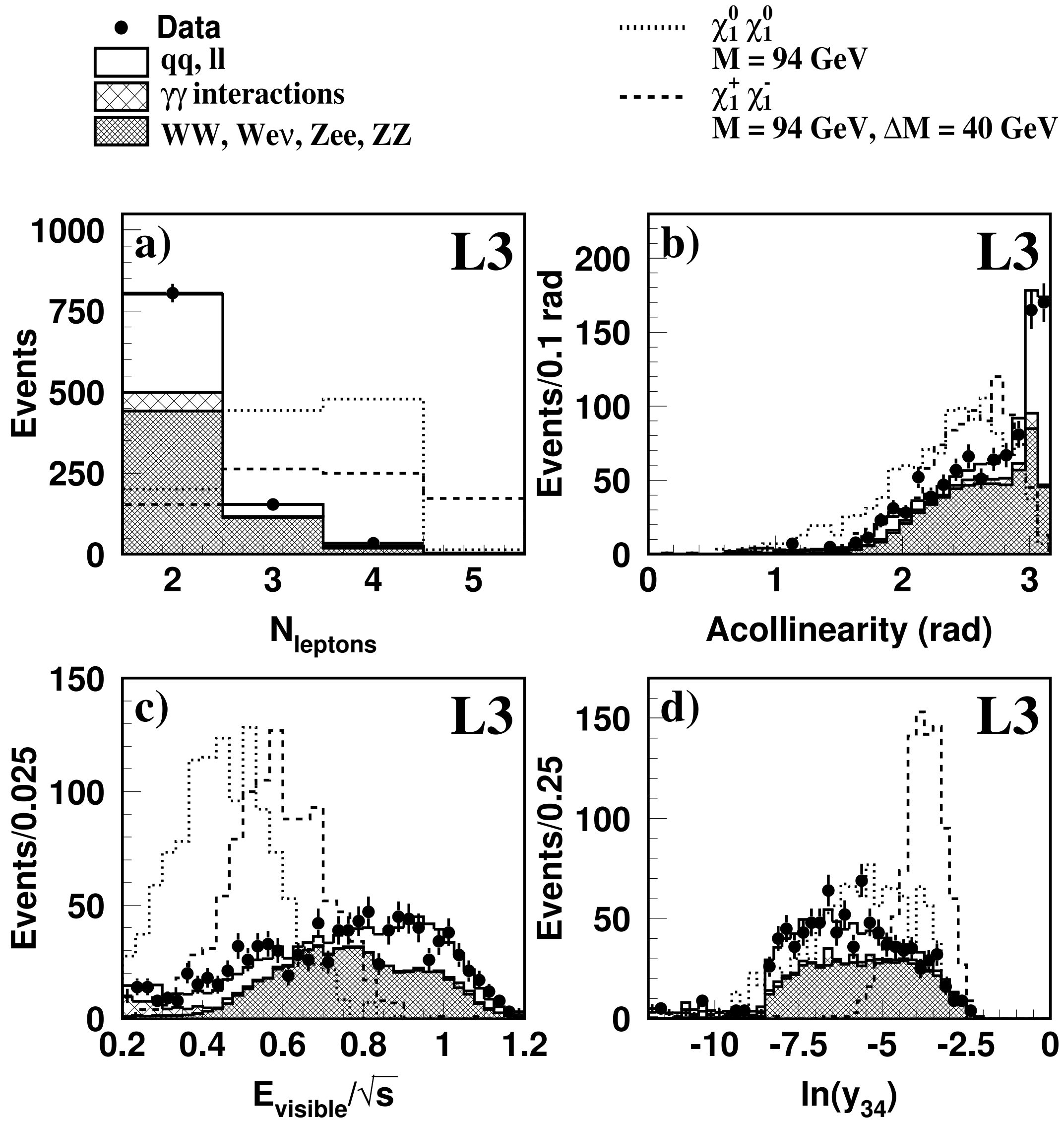

Figure 1: Data and Monte Carlo distributions of a) the number of leptons, b) acollinearity, c) the normalised visible energy and d) $\ln(y_{34})$ after the λ_{ijk} preselection. The solid histograms show the expectations for Standard Model processes at $\sqrt{s} = 189$ GeV. The dotted and dashed histograms show two examples of signal, with dominant coupling λ_{133}. The dotted histograms represent the process $\mathrm{e^+e^-} \rightarrow \tilde{\chi}^0_1\tilde{\chi}^0_1$, for $M_{\tilde{\chi}^0_1} = 94$ GeV, corresponding to five hundred times the luminosity of the data. The dashed ones represent $\mathrm{e^+e^-} \rightarrow \tilde{\chi}^+_1\tilde{\chi}^-_1$, with $M_{\tilde{\chi}^\pm_1} = 94$ GeV and $\Delta M = M_{\tilde{\chi}^\pm_1} - M_{\tilde{\chi}^0_1} = 40$ GeV, corresponding to twenty times the luminosity.

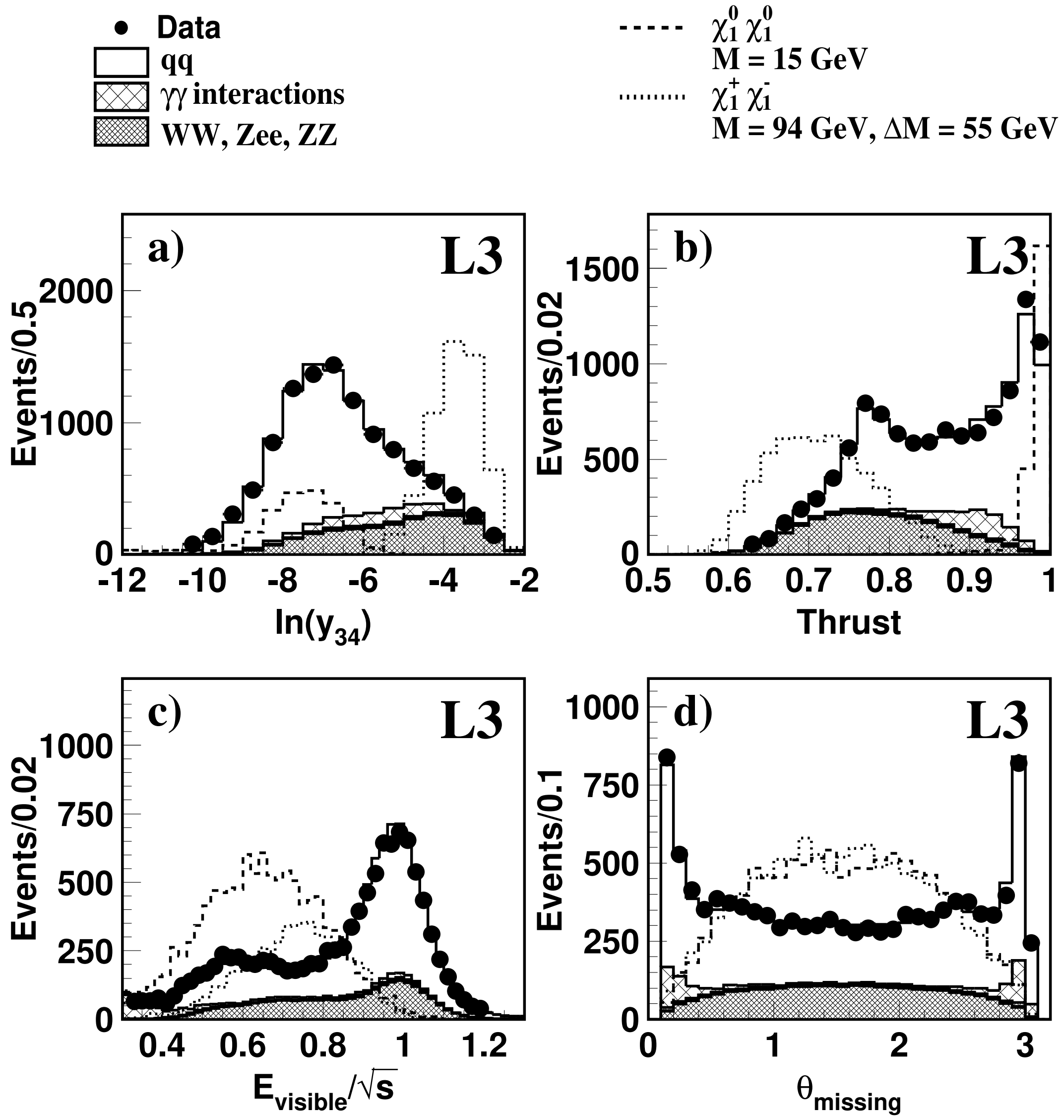

Figure 2: Data and Monte Carlo distributions of a) $\ln(y_{34})$, b) thrust, c) normalised visible energy and d) polar angle of the missing momentum after the λ'_{ijk} preselection. The solid histograms show the expectations for Standard Model processes at $\sqrt{s} = 189$ GeV. The dashed and dotted histograms show two examples of signal, with coupling λ'_{311}. The dashed histograms represent the process $\mathrm{e^+e^-} \rightarrow \tilde{\chi}^0_1\tilde{\chi}^0_1 \rightarrow$ 4 jets $\nu\bar{\nu}$, with $M_{\tilde{\chi}^0_1} = 15$ GeV, corresponding to thirty times the luminosity of the data. The dotted ones represent $\mathrm{e^+e^-} \rightarrow \tilde{\chi}^+_1\tilde{\chi}^-_1$, with $M_{\tilde{\chi}^\pm_1} = 94$ GeV and $\Delta M = M_{\tilde{\chi}^\pm_1} - M_{\tilde{\chi}^0_1} = 55$ GeV, with subsequent $\tilde{\chi}^0_1\tilde{\chi}^0_1$ decays into 4 jets $\nu\bar{\nu}$, corresponding to one hundred times the luminosity.

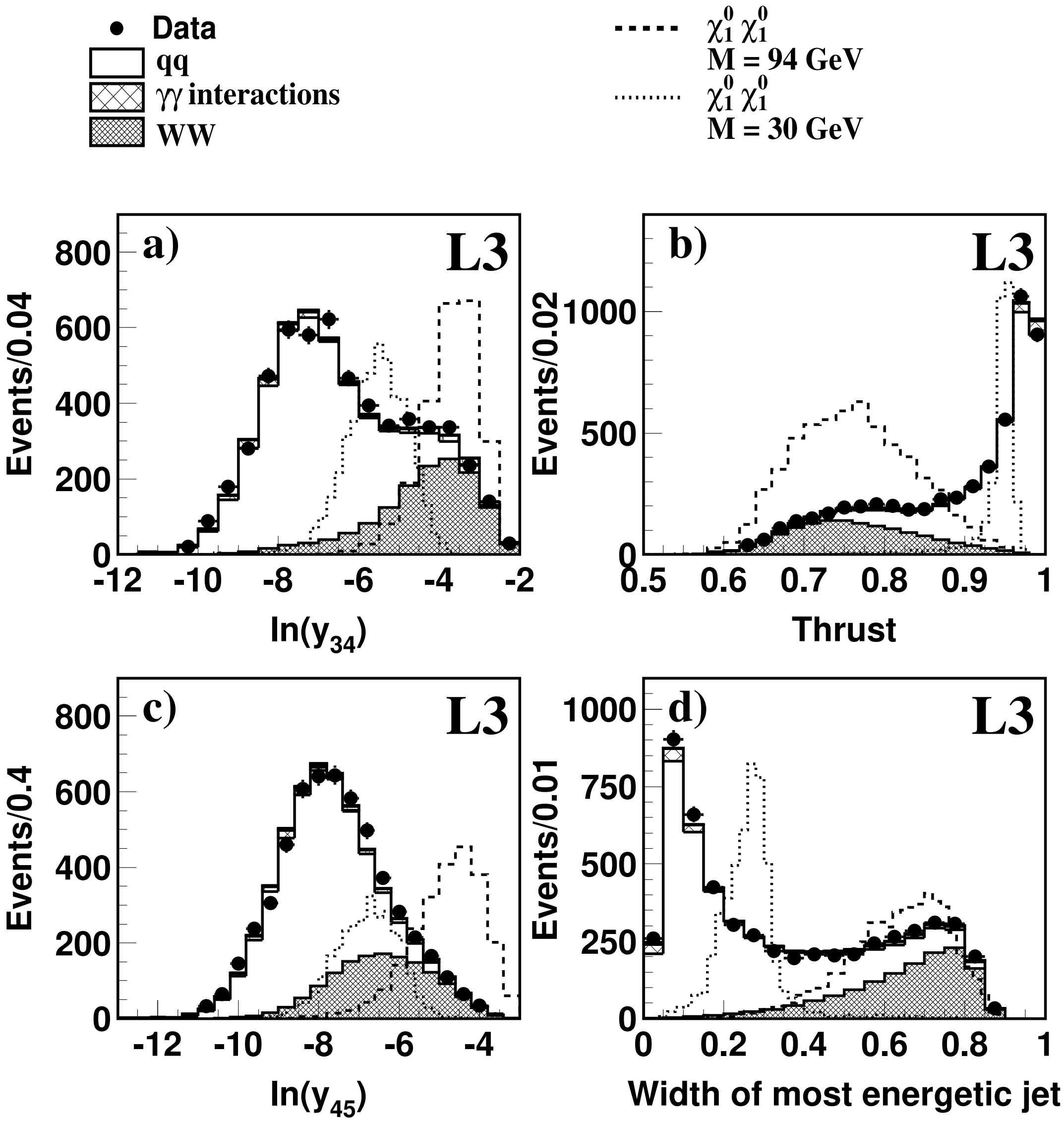

Figure 3: Data and Monte Carlo distributions of a) $\ln(y_{34})$, b) thrust, c) $\ln(y_{45})$ and d) width of the most energetic jet after the λ''_{ijk} preselection. The solid histograms show the expectations for Standard Model processes at $\sqrt{s} = 189$ GeV. The dashed and dotted histograms show two examples of signal, with dominant coupling λ''_{212}, corresponding to decays into c, d and s quarks. The dashed histograms represent the process $e^+e^- \rightarrow \tilde{\chi}_1^0\tilde{\chi}_1^0$, with $M_{\tilde{\chi}_1^0} = 94$ GeV, corresponding to one thousand times the luminosity of the data. The dotted ones represent the same process, with $M_{\tilde{\chi}_1^0} = 30$ GeV, corresponding to fifteen times the luminosity.

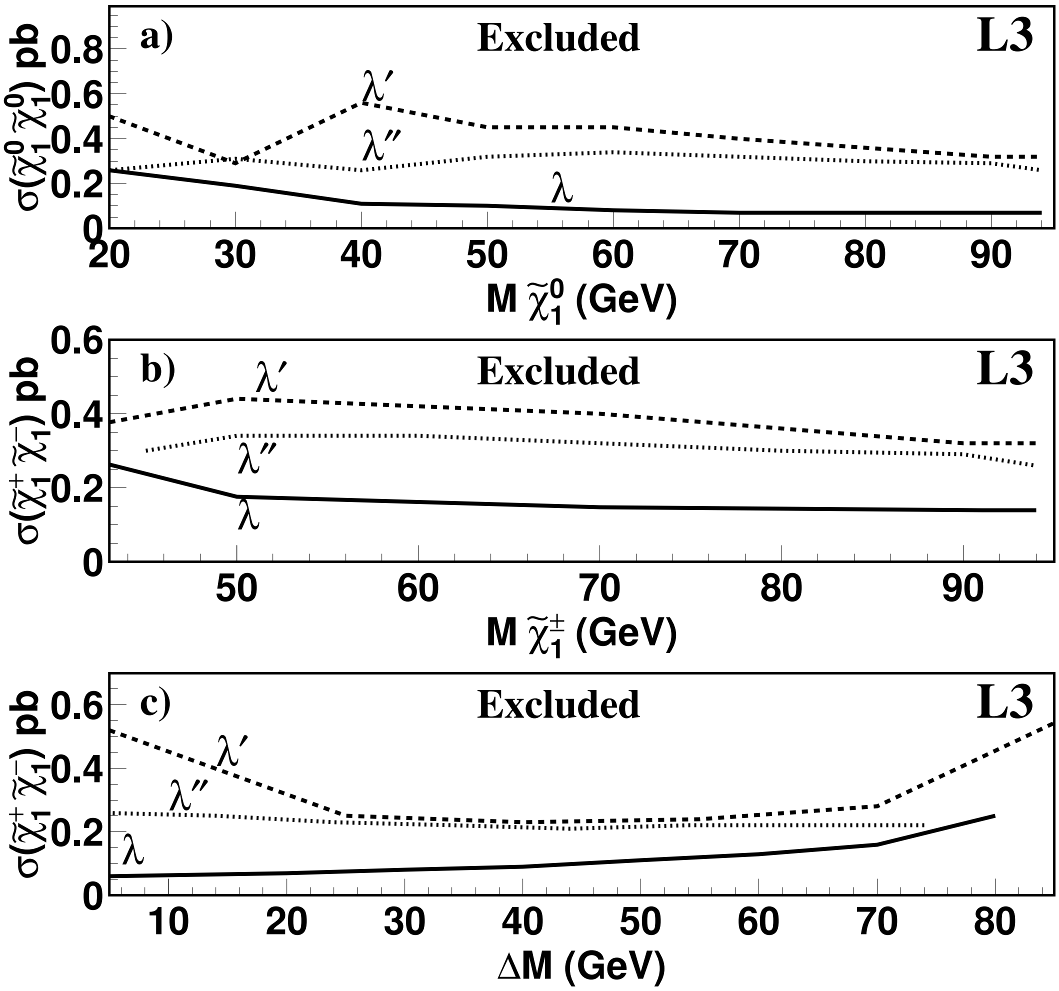

Figure 4: 95% C.L. upper limits on: a) the neutralino pair-production cross section as a function of the neutralino mass; the chargino pair-production cross section b) as a function of the chargino mass, in the direct decay mode and c) as a function of $\Delta M = M_{\tilde{\chi}_1^\pm} - M_{\tilde{\chi}_1^0}$, for $M_{\tilde{\chi}_1^\pm} = 94$ GeV, in the indirect decay mode. The solid lines show the limits obtained by the λ_{133} analysis, the dotted lines show those obtained by the λ'_{311} analysis and the dashed lines show those obtained by the λ''_{212} analysis.

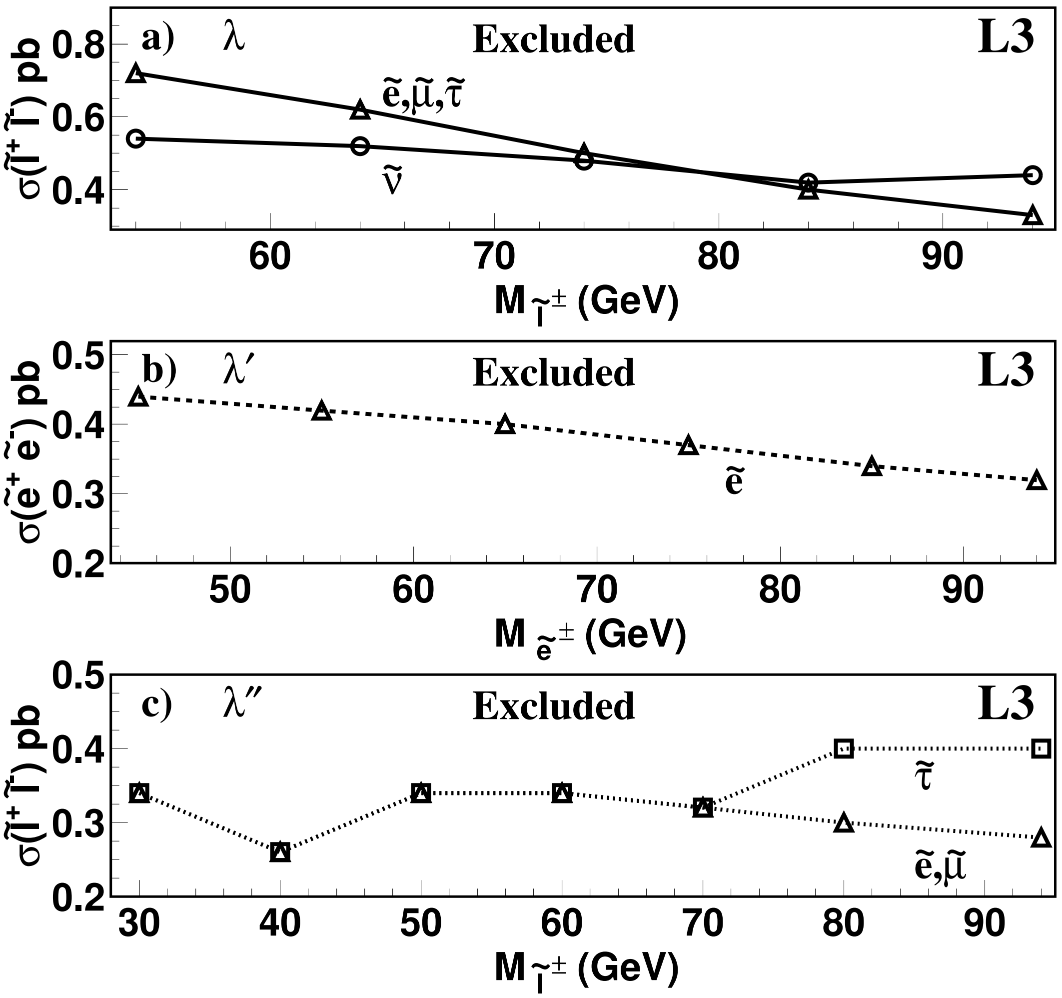

Figure 5: 95% C.L. upper limits on the scalar lepton pair-production cross section, in the direct decay mode, as a function of the scalar lepton mass for: a) λ_{ijk}, b) λ'_{ijk} and c) λ''_{ijk}. The solid lines show the limits obtained by the λ_{12k} analysis for scalar electrons, muons and taus and by the λ_{121} analysis for scalar neutrinos. The dashed line shows the limit obtained by the λ'_{311} analysis for scalar electrons. The dotted lines show those obtained by the λ''_{212} analysis for scalar electrons, muons and taus.

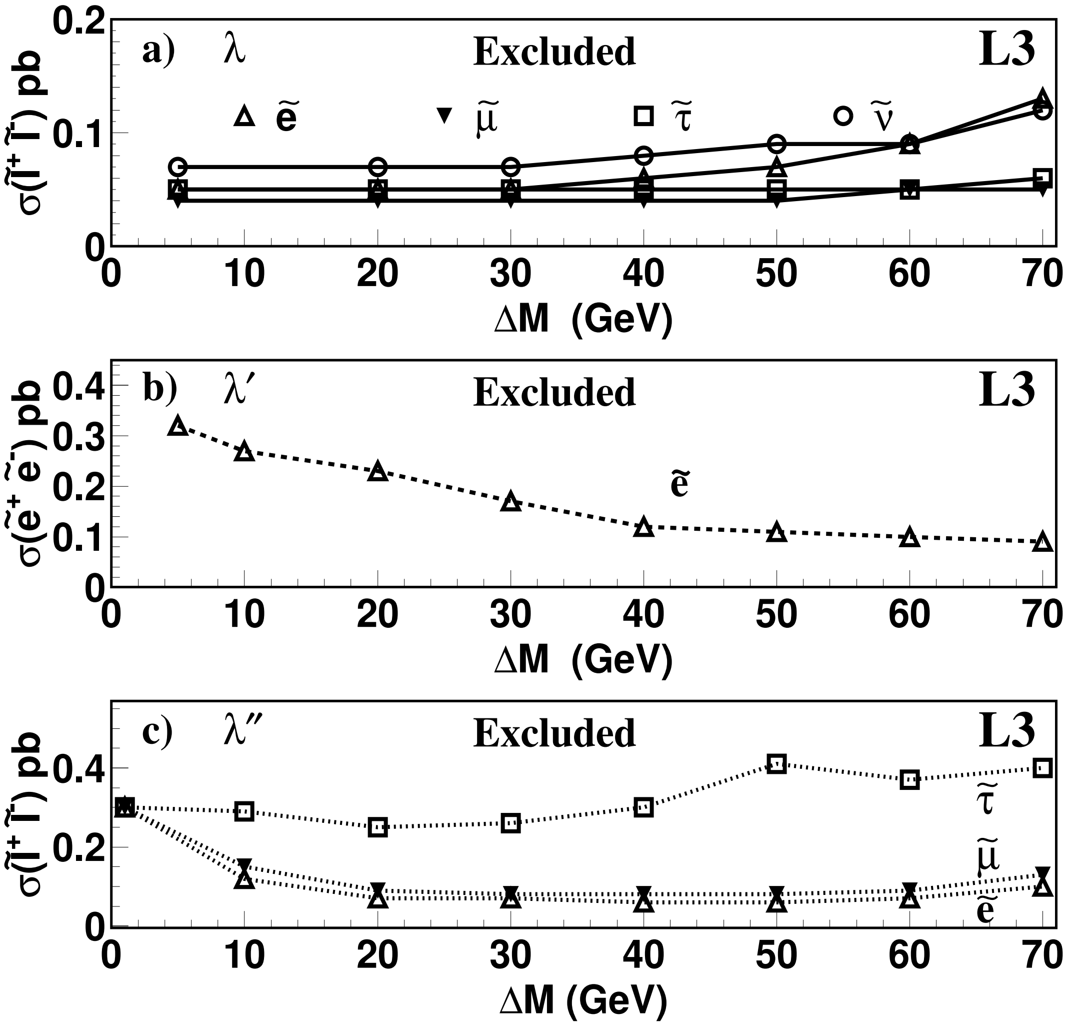

Figure 6: 95% C.L. upper limits on the scalar lepton pair-production cross section, in the indirect decay mode, for $M_{\tilde{\ell}_R} = 94$ GeV and as a function of $\Delta M = M_{\tilde{\ell}_R} - M_{\tilde{\chi}^0_1}$, for: a) λ_{ijk}, b) λ'_{ijk} and c) λ''_{ijk}. The solid lines show the limits obtained by the λ_{133} analysis for scalar leptons. The dashed line shows the limit obtained by the λ'_{311} analysis for scalar electrons. The dotted lines show those obtained by the λ''_{212} analysis for scalar electrons, muons and taus.

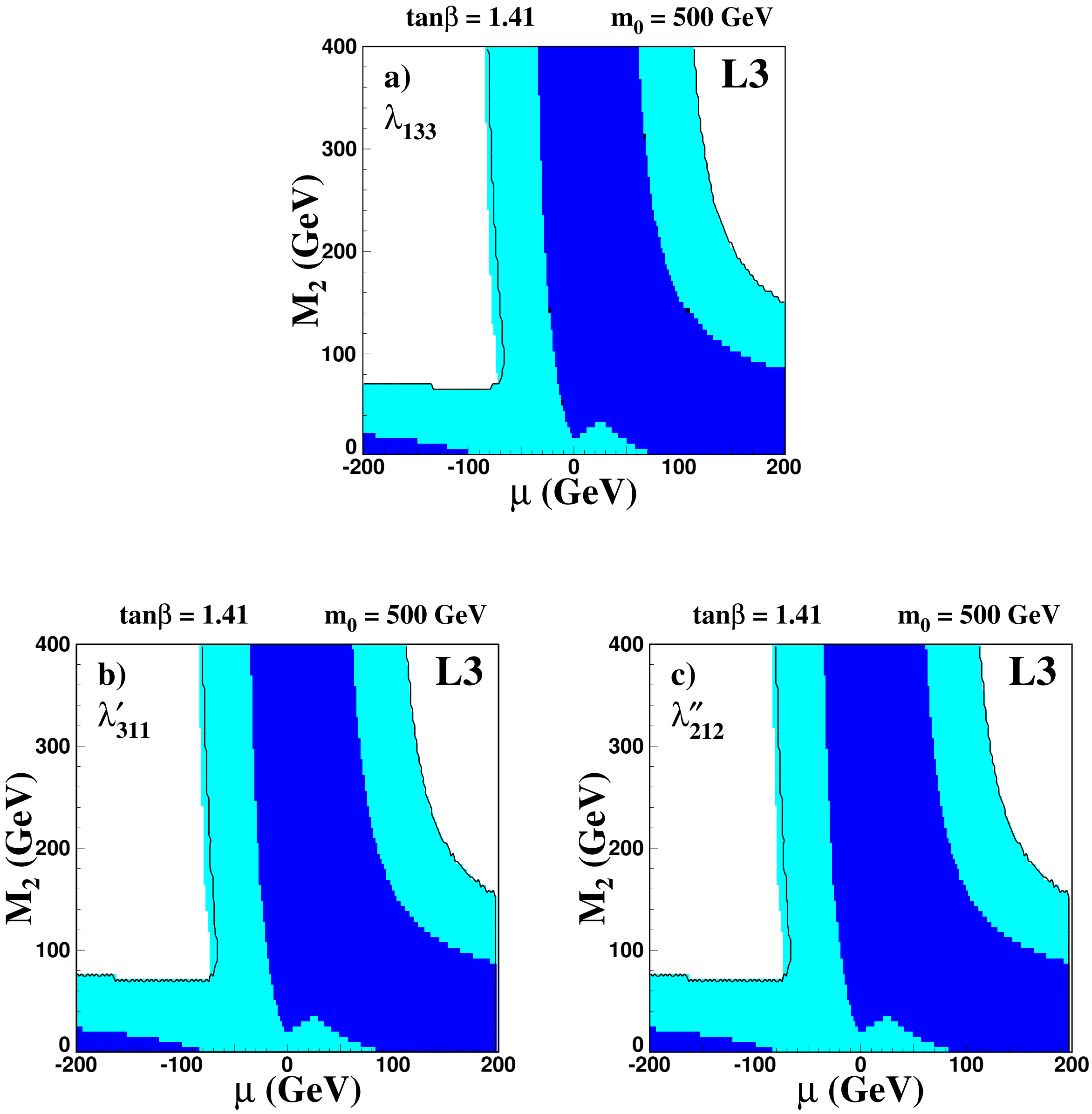

Figure 7: Exclusion regions at 95% C.L. for a) λ_{133}, b) λ'_{311} and c) λ''_{212}, for $\tan\beta = \sqrt{2}$ and $m_0 = 500$ GeV. The darker region is excluded by the Z lineshape measurements and the lighter region by the present analyses. The black solid lines indicate the chargino kinematic limit. The regions beyond the kinematic limit are excluded by neutralino analyses.

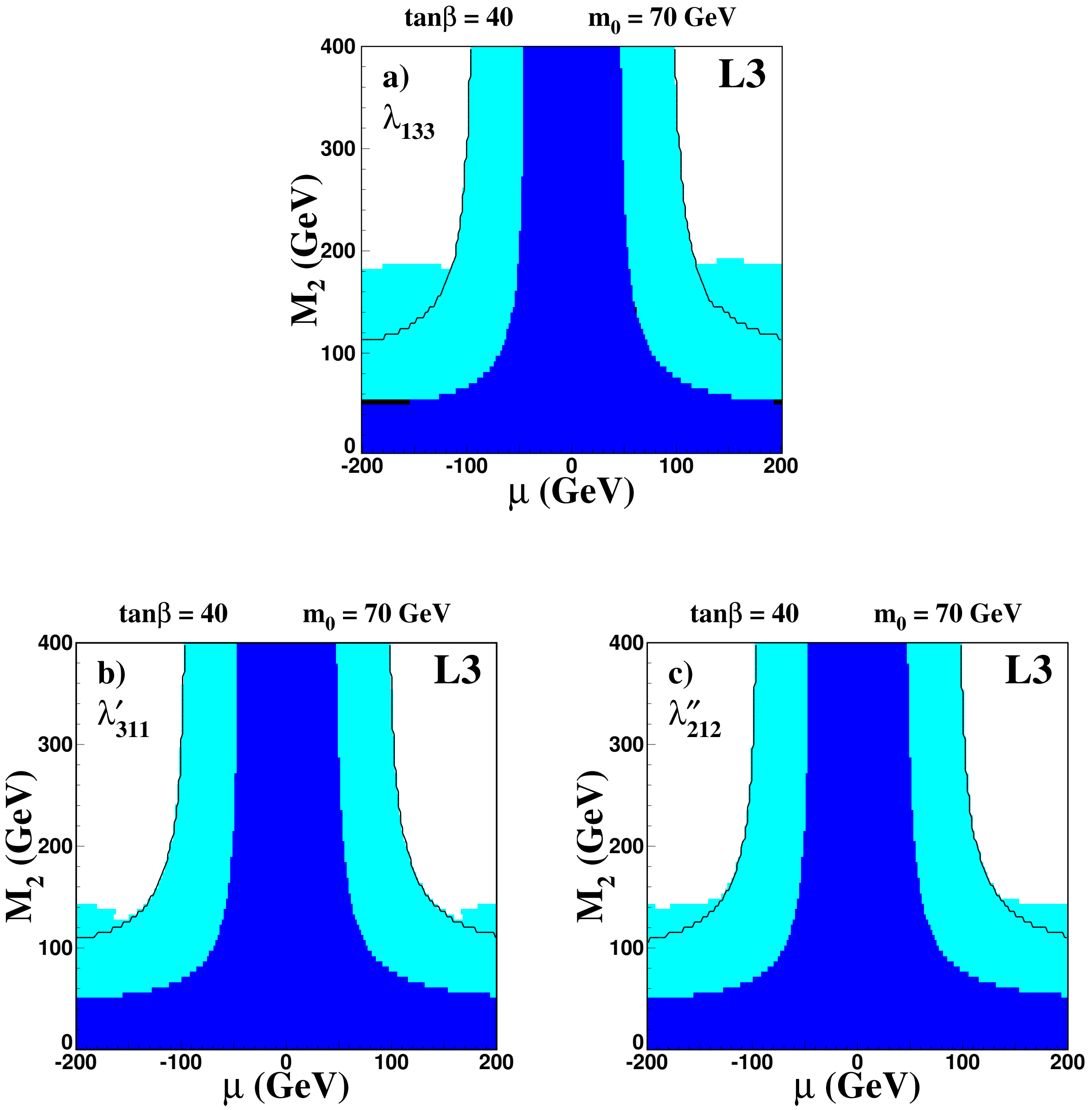

Figure 8: Exclusion regions at 95% C.L. for a) λ_{133}, b) λ'_{311} and c) λ''_{212}, for $\tan\beta = 40$ and $m_0 = 70$ GeV. The darker region is excluded by the Z lineshape measurements and the lighter region by the present analyses. The black solid lines indicate the chargino kinematic limit. The regions beyond the kinematic limit are excluded by neutralino analyses.

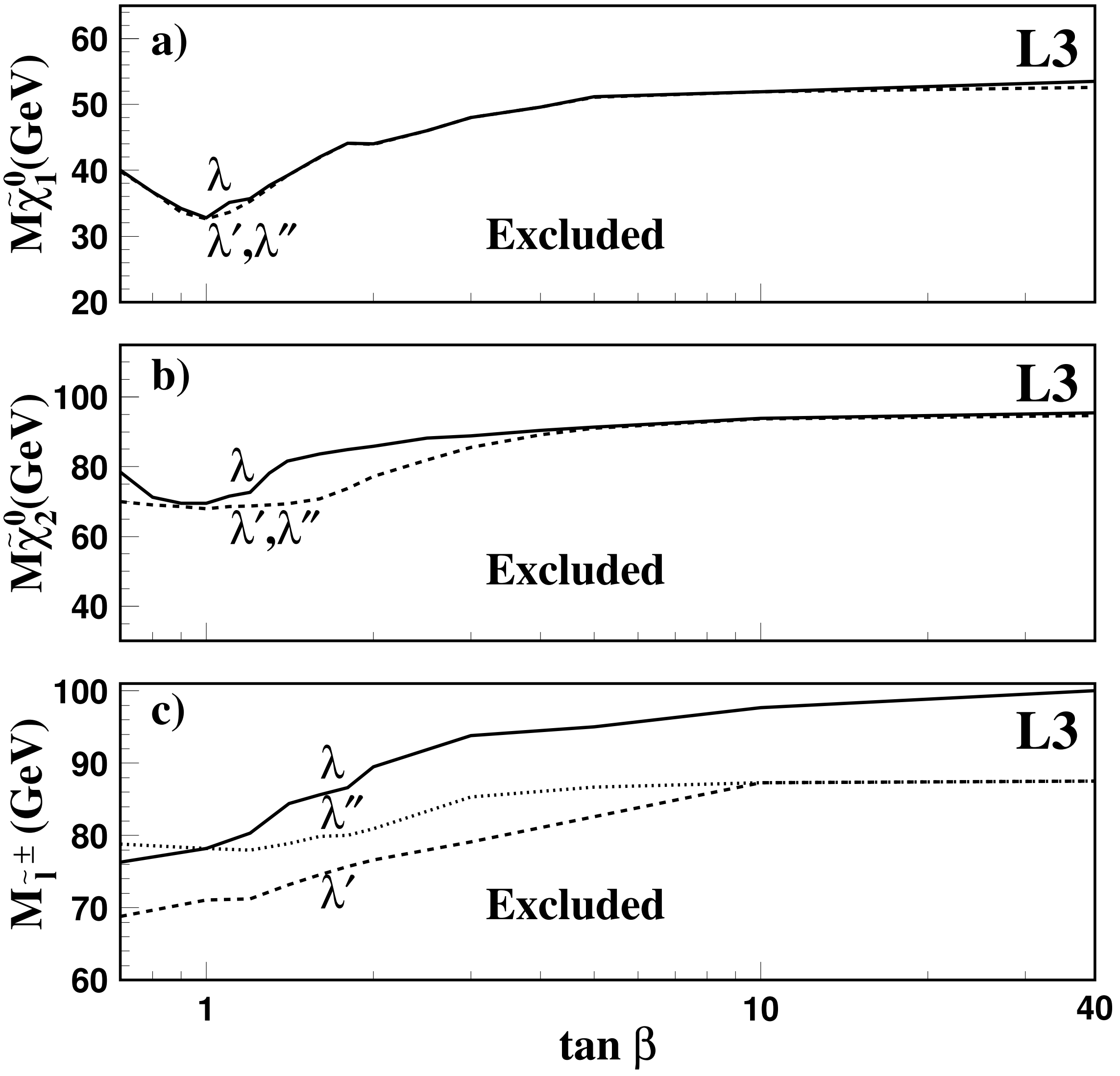

Figure 9: The solid, dashed and dotted lines, labelled with the corresponding coupling, show the 95% C.L. lower limits on the masses of a) $\tilde{\chi}^0_1$, b) $\tilde{\chi}^0_2$ and c) $\tilde{\ell}_R$, as a function of $\tan\beta$, for $0 \leq M_2 \leq 1000$ GeV and -500 GeV $\leq \mu \leq 500$ GeV. $m_0 =$ 500 GeV in a) and b) and $m_0 = 0$ in c).

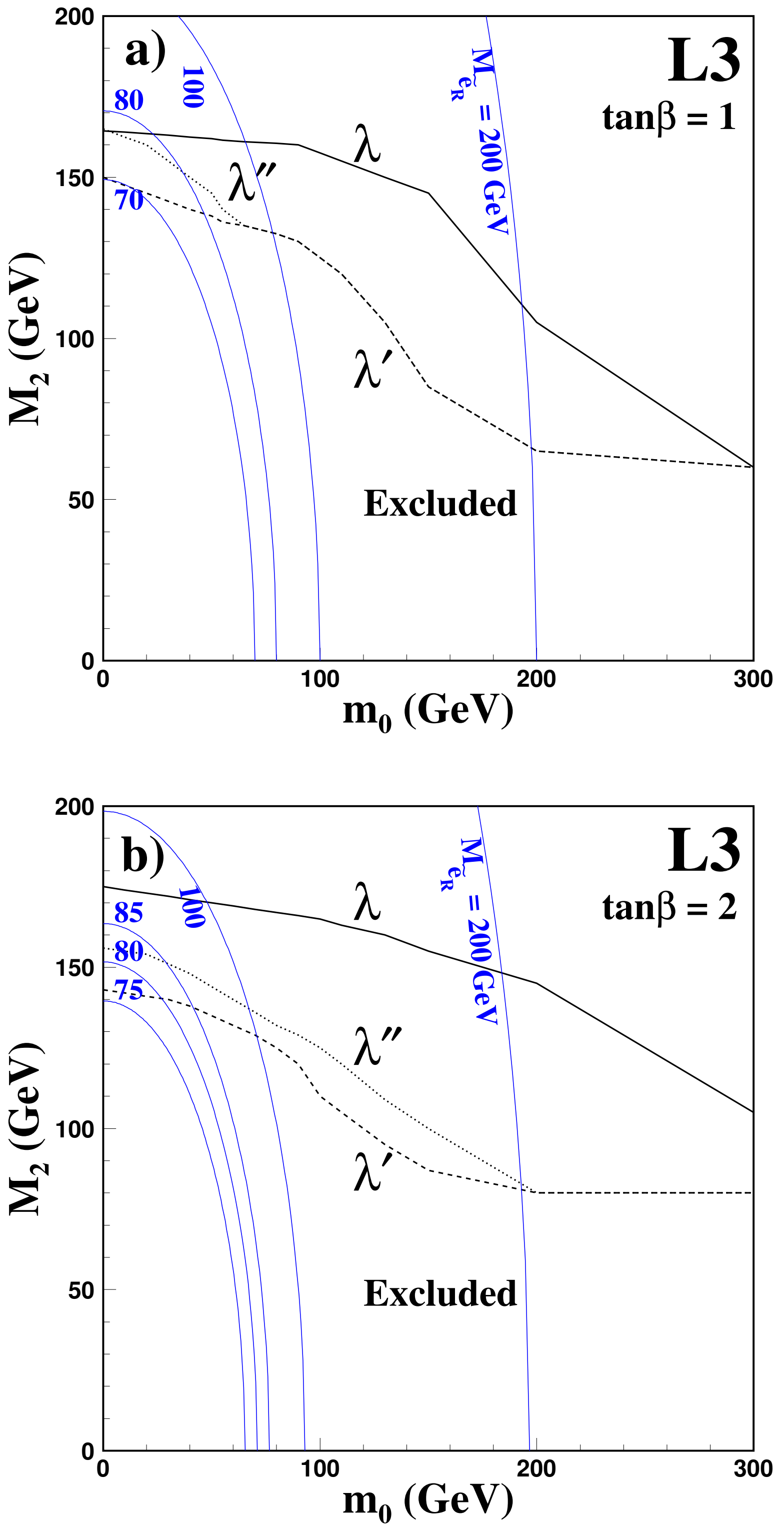

Figure 10: 95% C.L. exclusion contours in the $(M_2\,,\ m_0)$ plane, for $\mu\ <\ 0$ and $\tan\beta = 1$ (a) or $\tan\beta = 2$ (b). The lines labelled with the corresponding value in GeV represent the contours of constant scalar electron mass $M_{\tilde{e}_R}$. The solid, dotted and dashed curves show the 95% C.L. lower limits on M_2 as a function of m_0. The contributions from scalar lepton, neutralino and chargino searches are included.

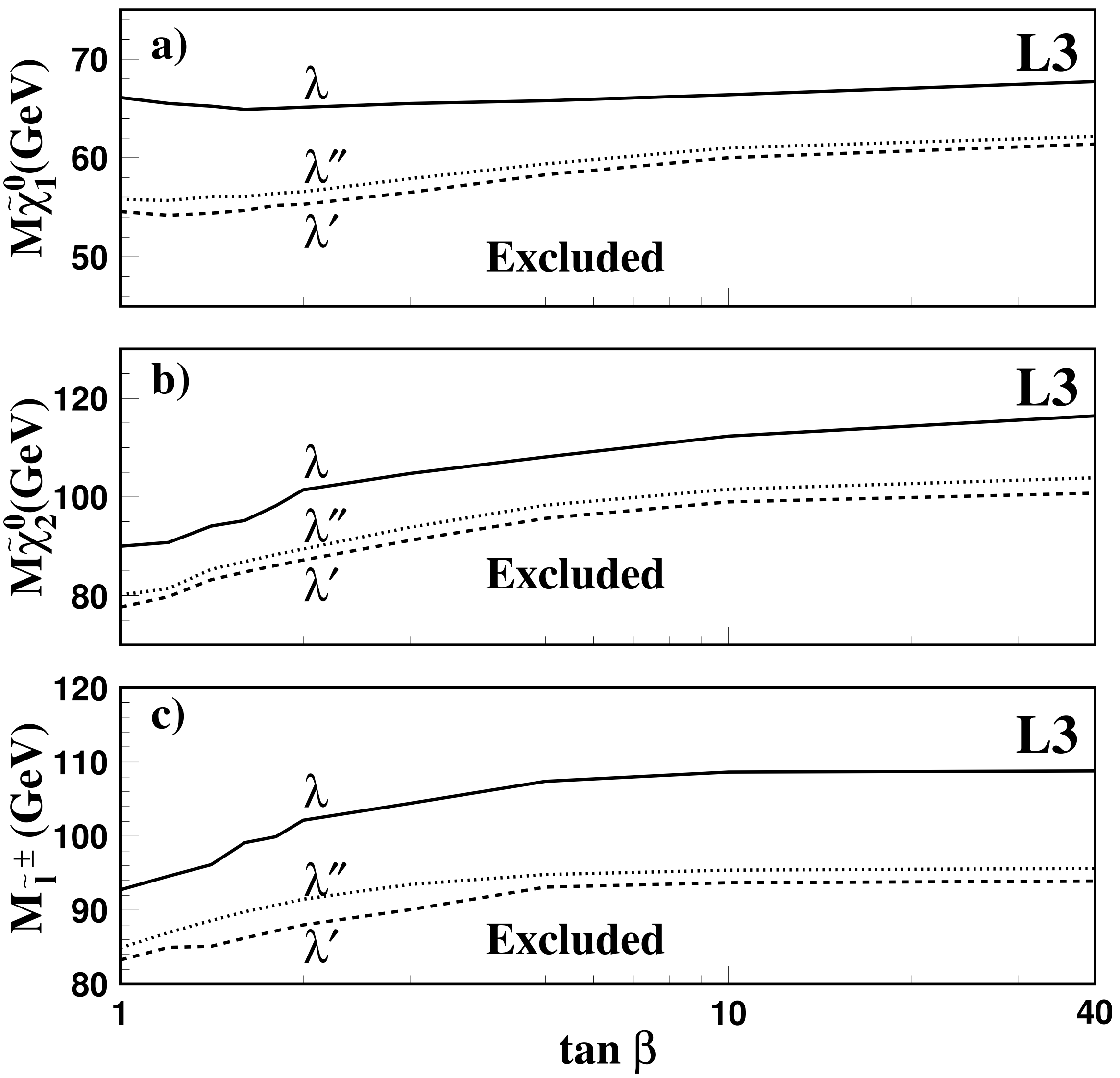

Figure 11: The solid, dashed and dotted lines, labelled with the corresponding coupling, show the 95% C.L. lower limits on the masses of a) $\tilde{\chi}^0_1$, b) $\tilde{\chi}^0_2$ and c) $\tilde{\ell}_R$, as a function of $\tan\beta$, for $0 \leq M_2 \leq 1000$ GeV, -500 GeV $\leq \mu \leq 500$ GeVand $m_0 = 50$ GeV.

A Selection details

Dedicated selections are performed to maximize *a priori* the analysis sensitivity $1/\sigma_{95}$, using Monte Carlo signal and background events, where σ_{95} is given by [25]:

$$\sigma_{95} = \frac{1}{\varepsilon} \sum_{n=0}^{\infty} c_n(b) P_b\,(n). \tag{4}$$

Here ε is the signal selection efficiency, $\mathrm{P}_b\,(n)$ is the Poisson probability to observe n events with an expected background of b events and $\mathrm{c}_n(b)$ are the 95% C.L. Bayesian upper limits on the signal expectation values.

In Tables 10 to 23 we summarize all selections. In addition to the variables described in Sections 4, 5 and 6, we apply cuts on the following variables:

- λ_{ijk}:
  - event thrust,
  - sum of the energies measured in the low angle calorimeters (Luminosity monitor and Active Lead Ring) covering the polar angle region between 1.5° and 9.0° ($E_{lum}+E_{alr}$),
  - energy in the electromagnetic (E_{bgo}) and hadronic calorimeters (E_{hcal}),
  - energy (E_n^{ℓ}) of the n identified leptons.
- λ'_{ijk}:
  - energy in a cone of 12° half-opening angle around the beam axis (E_{v12}),
  - sphericity,
  - probability ($Prob(\chi^2_{WW}, 5)$ or $Prob(\chi^2_{ZZ}, 5)$) that the reconstructed invariant mass, after a 5C fit, is consistent with $\mathrm{W^+W^-}$ or ZZ pair-production,
  - energy (E_{20}^{ℓ}) in a cone of 20° half-opening angle around the direction of the lepton candidate, calculated subtracting the lepton energy,
  - jet invariant masses (M_{jet1} and M_{jet2}).
- λ''_{ijk}:
  - jet widths
  - E_{20}^{ℓ}.

The cut values are chosen according to the procedure described above. In particular, the selection criteria for the variables marked with * are optimized simultaneously.

$\lambda_{ijk}:\ 4\ell + \not{E}$				
	Low mass values ($\leq$ 25 GeV)		High mass values ($\geq$ 25 GeV)	
	$\ell =$ e, μ only	$\ell = \tau$	$\ell =$ e, μ only	$\ell = \tau$
$N_{e,\mu}$	≥ 2	–	≥ 2	–
$N_{e,\mu,\tau}$	–	≥ 3	–	≥ 3
N_{tracks}	4	4 – 6	3 – 4	3 – 8
$N_{clusters}$	4 – 8	4 – 16	4 – 8	6 – 24
$E_{lum} + E_{alr}$ (GeV)	< 10	< 10	< 10	< 10
E_{bgo} (GeV)	< 150	> 20	< 100	–
E_{hcal} (GeV)	< 10	< 15	< 10	–
$E_{vis}/\sqrt{s}$	0.20 – 0.90	0.20 – 0.60	0.20 – 0.90	0.20 – 0.60
p^T_{miss} (GeV)	> 7	> 7	> 7	> 7
* *Thrust*	–	–	< 0.947	< 0.918
* $\sin(\theta_{miss})$	> 0.277	> 0.486	> 0.430	> 0.436
* θ_{acol} (rad)	< 3.107	< 3.135	< 3.035	< 2.952
* θ_{acop} (rad)	< 3.107	–	< 3.050	< 3.044
* y_{34}	0.0002 – 0.0018	0.0002 – 0.0020	> 0.00060	> 0.00056

Table 10: Cut values of the $4\ell + \not{E}$ selections, for final states with at least one τ or with $\ell =$ e, μ only. Topologies with four leptons plus missing energy result from neutralino, chargino and scalar neutrino decays, as detailed in Table 2. Different selection criteria are developed according to the mass values of the pair-produced supersymmetric particles.

λ_{ijk} : $2\ell + \not{E}$ and 6ℓ		
	$2\ell + \not{E}$	6ℓ
	$\ell =$ e, μ, τ	$\ell =$ e, μ, τ
$N_{e,\mu,\tau}$	$= 2$	≥ 4
N_{tracks}	$2 - 4$	$5 - 11$
$N_{clusters}$	$3 - 5$	$6 - 18$
N_{jets8}	$= 2$	$-$
$E_{lum} + E_{alr}$ (GeV)	< 10	< 10
E_{bgo} (GeV)	$-$	$15 - 125$
E_1^ℓ (GeV)	$30 - 60$	$-$
$E_1^\ell + E_2^\ell$(GeV)	> 40	$-$
$E_{vis}/\sqrt{s}$	$0.25 - 0.55$	$0.30 - 1.20$
p_{miss}^T (GeV)	> 7	> 7
* *Thrust*	$-$	< 0.971
* $\sin(\theta_{miss})$	> 0.278	> 0.314
* θ_{acol} (rad)	< 2.903	$-$
* θ_{acop} (rad)	< 2.904	$-$
* y_{34}	$-$	> 0.0009

Table 11: Selection criteria of the $2\ell + \not{E}$ and 6ℓ selections. Topologies with two leptons plus missing energy arise from chargino and scalar lepton direct decays, as shown in Table 2. Six lepton topologies result from chargino direct decays. Inclusive selection criteria are developed for final states with $\ell =$ e, μ or τ.

λ_{ijk} : $(\geq 4)\,\ell +$ (jets) $+\not\!\!E$, with $\ell =$ e, μ only							
	$\Delta M \leq 20$ GeV	$\Delta M = 20 - 50$ GeV			$\Delta M \geq 50$ GeV		
$N_{e,\mu}$	≥ 2	≥ 2			≥ 2		
$E_{lum} + E_{alr}$ (GeV)	< 10	< 10			< 10		
E_{bgo} (GeV)	< 110	< 110			< 110		
p^T_{miss} (GeV)	> 7	> 7			> 7		
* *Thrust*	< 0.961	<0.878			<0.811		
* $\sin(\theta_{miss})$	> 0.259	> 0.362			> 0.389		
* θ_{acol} (rad)	< 3.044	< 3.112			< 2.998		
* θ_{acop} (rad)	< 3.139	< 3.136			< 3.065		
* y_{34}	> 0.0026	> 0.0109			> 0.0118		
		hadronic	mixed	leptonic	hadronic	mixed	leptonic
N_{tracks}	$5 - 11$	$12 - 26$	$8 - 17$	$5 - 8$	$18 - 28$	$8 - 22$	$5 - 6$
$N_{clusters}$	$6 - 26$	$35 - 52$	$18 - 40$	$6 - 12$	$38 - 60$	$20 - 42$	$6 - 11$
$E_{vis}/\sqrt{s}$	0.30–0.90	0.50–0.85	0.40–0.85	0.35–0.75	0.60–0.90	0.45–0.80	0.30–0.75

Table 12: Cut values of the $(\geq 4)\,\ell+$ (jets) $+\not\!\!E$ selections, for final states with $\ell =$ e, μ only. Topologies with multileptons plus possible jets and missing energy result from neutralino, chargino and scalar lepton indirect decays, as presented in Table 2. Different selection criteria are developed depending on the mass differences $\Delta M = M_{\tilde{\chi}^\pm_1} - M_{\tilde{\chi}^0_1}$, $M_{\tilde{\chi}^0_n} - M_{\tilde{\chi}^0_1}$ or $M_{\tilde{\ell}_R} - M_{\tilde{\chi}^0_1}$. For large and medium ΔM three selections are applied according to the virtual W-pair decays into hadronic, mixed or leptonic final states.

$\lambda_{ijk}:\ (\geq 4)\,\ell+$ (jets) $+\not\!\!E$, with $\ell=\tau$			
	$\Delta M \leq 20$ GeV	$\Delta M \geq 20$ GeV	
$N_{e,\mu,\tau}$	≥ 3	≥ 3	
$E_{lum}+E_{alr}$ (GeV)	< 10	< 10	
p^T_{miss} (GeV)	> 7	> 7	
* *Thrust*	< 0.991	<0.832	
* $\sin(\theta_{miss})$	> 0.396	> 0.464	
* θ_{acol} (rad)	< 3.058	< 3.092	
* θ_{acop} (rad)	$-$	< 3.140	
* y_{34}	> 0.0018	> 0.0141	
		hadronic and mixed	leptonic
N_{tracks}	6 – 12	8 – 25	5 – 12
$N_{clusters}$	6 – 32	20 – 52	8 – 24
$E_{vis}/\sqrt{s}$	0.30–0.65	0.30–0.70	0.30–0.70

Table 13: Selection criteria of the $(\geq 4)\,\ell+$ (jets) $+\not\!\!E$ selections, for final states with at least one τ. Topologies with multileptons plus possible jets and missing energy arise from neutralino, chargino and scalar lepton indirect decays, as listed in Table 2. Different selection criteria are developed depending on the mass differences $\Delta M = M_{\tilde{\chi}^{\pm}_1} - M_{\tilde{\chi}^0_1}$, $M_{\tilde{\chi}^0_n} - M_{\tilde{\chi}^0_1}$ or $M_{\tilde{\ell}_R} - M_{\tilde{\chi}^0_1}$. For ΔM greater than 20 GeV, three selections are applied according to the virtual W-pair decays into hadronic and mixed or leptonic final states.

λ'_{ijk} : 4 jets $+2\tau$			
	Low masses ($\leq$ 30 GeV)	Medium masses (35–50 GeV)	High masses ($\geq$ 55 GeV)
E_{v12}/E_{vis}	< 0.20		
$E_{lum}+E_{alr}$ (GeV)	< 1		
W mass window	reject if 70 GeV$< M_{qq} <$ 95 GeV and 70 GeV$< M_{\ell\nu} <$ 90 GeV		
N_{tracks}	8–29	5–34	13–38
$N_{clusters}$	16–63	24–73	43–94
N_{jets8}	–	–	≥ 4
$N_{e,\mu,\tau}$	≥ 1	≥ 1	≥ 2
$E_{miss}/\sqrt{s}$	< 0.33	< 0.35	< 0.24
$Prob(\chi^2_{WW},5)$	–	< 0.5	< 0.3
$Prob(\chi^2_{ZZ},5)$	–	–	< 0.3
Sphericity	0.003–0.3	< 0.42	0.1–0.81
W_{jet1}	0.04–0.36	≥ 0.1	≥ 0.1
W_{jet2}	0.04–0.36	≥ 0.1	–
$\lvert M_{jet1}-M_{jet2}\rvert$ (GeV)	<24	–	–
θ_{acol} (rad)	–	<3.09	–
$E_{bgo}/\sqrt{s}$	0.1–0.7	0.2–0.6	0.2–0.6
$E_{hcal}/\sqrt{s}$	0.05–0.4	0.05–0.3	0.05–0.35
* *Thrust*	0.94–0.99	0.83–0.98	0.61–0.83
* $\ln(y_{34})$	> -6.18	> -5.55	> -4.73
* $\sin(\theta_{miss})$	> 0.24	> 0.67	> 0.66
* $E_{vis}/\sqrt{s}$	0.59–0.89	0.67–0.95	0.69–0.88
* θ_{acop} (rad)	< 3.139	<3.093	< 3.136

Table 14: Values of the selection requirements for the "4 jets + 2 taus" selections. These final states arise from neutralino decays via λ' coupling, as shown in Table 5.

λ'_{ijk} : 4 jets $+ \tau + \not{E}$			
	Low masses ($\leq$ 30 GeV)	Medium masses (35–50 GeV)	High masses ($\geq$ 55 GeV)
E_{v12}/E_{vis}	< 0.20		
$E_{lum} + E_{alr}$ (GeV)	< 1		
$N_{e,\mu,\tau}$	≥ 1		
W mass window	reject if 70 GeV$< M_{qq} <$ 95 GeV and 70 GeV$< M_{\ell\nu} <$ 90 GeV		
N_{tracks}	5–29	6–38	19–42
$N_{clusters}$	15–65	20–77	43–97
$E_{miss}/\sqrt{s}$	<0.37	<0.42	0.08–0.34
$Prob(\chi^2_{WW}, 5)$	<0.8	<0.16	<0.17
$Prob(\chi^2_{ZZ}, 5)$	<0.4	–	<0.5
Sphericity	<0.2	<0.46	0.08–0.8
W_{jet1}	0.03–0.4	0.04–0.65	≥ 0.2
W_{jet2}	0.03–0.5	0.04–0.65	≥ 0.05
$\lvert M_{jet1} - M_{jet2} \rvert$ (GeV)	<28	–	–
$E_{bgo}/\sqrt{s}$	0.1–0.66	0.13–0.66	0.21–0.56
$E_{hcal}/\sqrt{s}$	0.03–0.41	0.03–0.41	<0.40
* *Thrust*	0.95–0.99	0.84–0.99	0.60–0.85
* $\ln(y_{34})$	> -7.54	> -6.74	> -4.89
* $\sin(\theta_{miss})$	>0.35	>0.68	>0.47
* $E_{vis}/\sqrt{s}$	0.63–0.92	0.67–0.84	0.62–0.82
* θ_{acop} (rad)	<3.05	<3.02	–

Table 15: Cut values of the "4 jets $+ \tau + \not{E}$" selections. These final states arise from neutralino decays via λ' coupling, as detailed in Table 5.

λ'_{ijk} : 4 jets + $\not{E}$			
	Low masses ($\leq$ 30 GeV)	Medium masses (35–50 GeV)	High masses ($\geq$ 55 GeV)
E_{v12}/E_{vis}	< 0.20		
$E_{lum} + E_{alr}$ (GeV)	< 1		
N_{jets8}	–	–	≥ 3
$N_{e,\mu,\tau}$	≥ 1		
W mass window	reject if 70 GeV$< M_{qq} <$ 95 GeV and 70 GeV$< M_{\ell\nu} <$ 90 GeV		
N_{tracks}	4–31	6–33	14–41
$N_{clusters}$	10–64	18–74	43–99
$E_{miss}/\sqrt{s}$	<0.41	<0.41	0.08–0.43
$Prob(\chi^2_{WW}, 5)$	–	–	<0.1
Sphericity	<0.3	<0.52	0.05–0.78
W_{jet1}	0.02–0.4	0.04–0.65	≥ 0.35
W_{jet2}	0.01–0.6	0.04–0.75	≥ 0.07
$\|M_{jet1} - M_{jet2}\|$ (GeV)	<25	–	–
$E_{bgo}/\sqrt{s}$	0.08–0.57	0.11–0.57	0.11–0.57
$E_{hcal}/\sqrt{s}$	0.04–0.42	0.02–0.37	0.02–0.37
* *Thrust*	>0.95	0.91–0.97	0.55–0.92
* $\ln(y_{34})$	> -8.63	> -6.40	> -4.74
* $\sin(\theta_{miss})$	>0.66	>0.47	>0.62
* $E_{vis}/\sqrt{s}$	0.61–0.80	0.35–0.79	0.35–0.79
* θ_{acop} (rad)	<3.07	<3.05	<3.

Table 16: Values of the selection requirements for the "4 jets + $\not{E}$" selections. These final states follow from neutralino decays via λ' coupling, as listed in Table 5.

λ'_{ijk} : multijets + leptons			
$N_{clusters}$	≥ 13		
N_{tracks}	≥ 10		
E_{v12}/E_{vis}	< 0.30		
$\sin(\theta_T)$	>0.139		
E_{par}/E_{vis}	<0.5		
E_{perp}/E_{vis}	<0.2		
N_{jets8}	≥ 3		
$E_{vis}/\sqrt{s}$	≥ 0.7		
$\sin(\theta_{miss})$	>0.139		
$N_{e,\mu}$	≥ 2, one isolated ($E^{\ell}_{20} < 1$ GeV, $E_{lepton} > 5$ GeV)		
$M_{\tilde{\chi}^{\pm}_1}$ (GeV)	50	60	≥ 70
* *Thrust*	0.82–0.89	0.74–0.88	0.51–0.79
* $\ln(y_{34})$	> -5.56	> -5.22	> -5.80
* $\ln(y_{45})$	> -5.97	> -5.66	> -5.24

Table 17: Cut values for λ'_{ijk} chargino selections with a multijet topology with at least 2 leptons and no missing energy, as detailed in Table 5. Different selection criteria are developed according to the mass values of the pair–produced charginos.

λ'_{ijk} : multijets + $\not{E}$			
$N_{clusters}$	≥ 13		
N_{tracks}	≥ 10		
E_{v12}/E_{vis}	< 0.30		
$\sin(\theta_T)$	>0.139		
E_{par}/E_{vis}	<0.5		
E_{perp}/E_{vis}	<0.2		
N_{jets8}	≥ 3		
$E_{vis}/\sqrt{s}$	0.5–0.9		
$\sin(\theta_{miss})$	>0.436		
events with one isolated lepton ($E^{\ell}_{20} < 1$ GeV) are rejected			
$M_{\tilde{\chi}^{\pm}_1}$ (GeV)	50	60	≥ 70
* *Thrust*	0.82–0.90	0.71–0.84	0.54–0.80
* $\ln(y_{34})$	> -5.68	> -5.70	> -4.56
* $\ln(y_{45})$	> -6.17	> -5.94	> -5.21
* p^T_{miss}	> 10 GeV	> 20 GeV	> 20 GeV

Table 18: Selection criteria for λ'_{ijk} chargino selections with a multijet topology, missing energy and no isolated leptons, as presented in Table 5. Different selection criteria are developed according to the mass values of the pair–produced charginos.

λ'_{ijk} : multijets + lepton(s) and $\not{E}$	
$N_{clusters}$	≥ 13
N_{tracks}	≥ 10
E_{v12}/E_{vis}	< 0.30
$\sin(\theta_T)$	>0.139
E_{par}/E_{vis}	<0.5
E_{perp}/E_{vis}	<0.2
N_{jets8}	≥ 3
$E_{vis}/\sqrt{s}$	<0.9
$\sin(\theta_{miss})$	>0.436
$N_{e,\mu}$	≥ 1, one isolated ($E^{\ell}_{20} < 1$ GeV, $E_{lepton} < 30$ GeV)
W mass window	reject if 70 GeV$< M_{qq} <$ 90 GeV and 70 GeV$< M_{\ell\nu} <$ 90 GeV
* *Thrust*	0.56–0.87
* $\ln(y_{34})$	> -5.35
* $\ln(y_{45})$	> -6.22
* p^T_{miss}	> 12.3 GeV

Table 19: Values of the selection requirements for λ'_{ijk} chargino selections with a multijet topology with both lepton(s) and missing energy.

λ'_{ijk} : scalar electrons	
$N_{clusters}$	≥ 13
N_{tracks}	≥ 1
$E_{vis}/\sqrt{s}$	> 0.70
E_{perp}/E_{vis}	< 0.20
E_{par}/E_{vis}	< 0.20
E_{v12}/E_{vis}	< 0.30
E_{bgo}/E_{vis}	$0.05 - 0.98$
$\sqrt{s'}/\sqrt{s}$	> 0.80
$\sin(\theta_T)$	> 0.139
Thrust	< 0.95
$\ln(y_{34})$	> -8.0
$\ln(y_{45})$	> -9.0
N_e	≥ 1
E^{ℓ}_1 (GeV)	> 5

Table 20: Selection criteria of the scalar electron selections, for final states with 4 jets, 2 to 4 leptons and possible missing energy, as shown in Table 5.

λ''_{ijk} : multijets					
$N_{clusters}$	≥ 13				
N_{tracks}	≥ 1				
$E_{vis}/\sqrt{s}$	> 0.70				
E_{perp}/E_{vis}	< 0.20				
E_{par}/E_{vis}	< 0.20				
E_{v12}/E_{vis}	< 0.30				
E_{bgo}/E_{vis}	$0.05 - 0.98$				
$\sqrt{s'}/\sqrt{s}$	> 0.80				
$\sin(\theta_T)$	> 0.139				
$M_{\tilde{\chi}}$(GeV)	$20 - 30$	$30 - 40$	$40 - 50$	$50 - 60$	≥ 60
* *Thrust*	$0.940 - 0.973$	$0.901 - 0.960$	$0.828 - 0.919$	$0.755 - 0.889$	$0.575 - 0.844$
* $\ln(y_{34})$	> -5.85	> -5.70	> -5.20	> -5.16	> -4.77
* $\ln(y_{45})$	> -9.68	> -7.02	> -6.16	> -5.82	> -4.62
* W_{jet1}	$0.12 - 0.22$	$0.15 - 0.45$	$0.25 - 0.55$	$0.21 - 0.67$	$0.38 - 0.90$

Table 21: Cut values of the neutralino selections, for final states with at least six hadronic jets. The same multijet topologies arise from indirect neutralino and chargino hadronic decays, as presented in Table 6. Different selection criteria are developed according to the mass values of the pair-produced supersymmetric particles.

λ''_{ijk} : multijets + lepton(s)		
$N_{clusters}$	≥ 13	
E_{v12}/E_{vis}	< 0.20	
E_{bgo}/E_{vis}	0.05–0.98	
$\sin(\theta_T)$	>0.139	
	semileptonic	leptonic
E_{par}/E_{vis}	< 0.3	< 0.5
E_{perp}/E_{vis}	< 0.3	< 0.5
N_{tracks}	> 20	10–30
$N_{e,\mu,\tau}$	≥ 1	≥ 2
E^{ℓ}_{20}	> 1 GeV	–
* *Thrust*	0.52–0.83	0.55–0.79
* $\ln(y_{34})$	> -4.55	> -4.15
* $\ln(y_{45})$	> -5.02	> -4.58
* $\sin(\theta_{miss})$	> 0.24	> 0.51
* $E_{vis}/\sqrt{s}$	> 0.6	0.52–0.88

Table 22: Details of final selections for semileptonic and leptonic decays channels of the charginos for the λ'' coupling, as listed in Table 6.

λ''_{ijk} : scalar leptons	
$\tilde{\mathrm{e}}_R$	2 electrons. For at least one of them: $E^{\ell}_{20} > 1$ GeV
$\tilde{\mu}_R$	2 muons. For at least one of them: $E^{\ell}_{20} > 1$ GeV
$\tilde{\tau}_R$	1 lepton (e, μ, τ)
$\tilde{\tau}_R$ with high ΔM	1 lepton (e, μ, τ) and $M_{5C} = M_{\tilde{\tau}_R} \pm 5$ GeV.

Table 23: Cut values, in addition to the "multijets" requirements, of the scalar lepton selections (Table 21), for final states with 6 jets and 2 leptons, as shown in Table 6. Different selection criteria are developed according to the lepton flavour expected in the final state.